

November 23, 2022

The Role of Cytonemes and Diffusive Transport in the Establishment of Morphogen Gradients

Jay Stotsky^{1,*}, Hans Othmer¹¹ School of Mathematics, University of Minnesota, Minneapolis, MN, USA

Contents

1	Introduction and background	2
2	Cytoneme-based transport	4
2.1	Producer-initiated transport	4
2.2	Receiver-initiated transport	6
2.3	Cytoneme return rates and first-passage-time distributions	9
3	Stochastic models of cytoneme-based transport	11
3.1	Multiple cytonemes	12
3.2	Composite random processes	14
3.3	Stochastic simulations	16
3.4	Cell saturation effects	20
4	Transport in complex environments	22
4.1	Microscale to Macroscale	23
4.1.1	Limit equations	24
4.2	Comparison of diffusion and cytonemes	26
4.2.1	Diffusive transport	26
4.2.2	Transport via PIT cytonemes	28
5	Discussion	30
6	Acknowledgments	31
7	Appendices	33
7.1	Computation of FPT for cytonemes with a resting phase	33
7.2	Simplification of double sum for the composite process	34

Abstract

Spatial distributions of morphogens provide positional information in developing systems, but how the distributions are established and maintained remains an open problem. Transport by diffusion has been the traditional mechanism, but recent experimental work has shown that cells can also communicate by filopodia-like structures called cytonemes that make direct cell-to-cell contacts. Here we investigate the roles each may play individually in a complex tissue and how they can jointly establish a reliable spatial distribution of a morphogen.

1 Introduction and background

Pattern formation in embryonic development is a major, yet poorly understood, process in developmental biology. Throughout early development, maternal and zygotic cues regulate gene expression, cell proliferation, and differentiation in space and time in a highly-reproducible manner. Various theories have been proposed to explain how individual cells in an aggregate of essentially identical cells differentiate into a collection of different cell types organized into the appropriate spatial pattern in response to factors called morphogens. The analysis of models of how the spatiotemporal distribution of morphogens can be controlled so as to produce the appropriate cell type at the correct location in a tissue is an area in which mathematical modeling has led to significant insights [32]. There are currently two major theories of morphogen-based pattern formation: Turing's theory [44] and the theory of positional information. In Turing's theory patterns arise from the interaction of reaction and transport by diffusion without external cues. This can explain certain patterns such as spots on insects, but is less useful when the spatial pattern is determined by a specified distribution of morphogens, and here the theory of positional information due to Child [7] and Wolpert [48] is more appropriate.

In positional-information mechanisms of morphogen-mediated patterning, cells determine their spatial position by sensing the local levels of a spatially-graded morphogen, often produced at the boundary of a region to be patterned. The simplest model of how this functions is embodied in the French flag problem, which is to subdivide a finite interval $[0, L]$ on the x -axis into three equal partitions, the first to be colored blue, the second white, and the third red. This is accomplished by producing a morphogen at the left boundary, the distribution of which then evolves via diffusive transport and first-order decay in the interior, and removal at the right boundary. This leads to a monotone-decreasing gradient of the morphogen level. The interpretation of the gradient involves two thresholds that then lead to the appropriate coloration of the interval. This mechanism has gained widespread appeal for interpreting the appearance of different cell types in an initially-unstructured tissue such as the *Drosophila* wing disc [41], but it also raises numerous questions, such as how does the mechanism cope with tissues of different sizes [45].

Both Turing's theory and the theory of positional information rely on diffusion as the means of transport [27, 41] but other means of communication in tissues have been discovered in recent years, and the one of interest here uses what are called cytonemes. Cytonemes are rod-like structures similar to filopods, which extend from a cell by polymerizing actin at the tip. They are $\mathcal{O}(0.1-0.5)\mu\text{m}$ in diameter and up to $100\mu\text{m}$ in length. In the *Drosophila* wing disc they can be as long as $80\mu\text{m}$ which spans the entire length of the disc at early stages [33]. As with filopodia, cytonemes contain an actin network, but in addition, some contain myosin motors such as Myo-10 that can step along actin filaments to transport cargo [17]. Connections between a cytoneme and a cell, or directly between cytonemes, leads to three forms of communication between cells, as shown in Figure 1. The first method, shown in panel (A), is used in vertebrates to transfer the morphogen Wnt from producers to receivers, and we call this producer-induced transport (PIT). In this mode a morphogen-producing cell extends a cytoneme that attaches to a receiver cell and transfers a bolus of morphogen to the receiver. In some cases there may be successive transfers of morphogen-filled vesicle-like structures carried along the cytoneme by molecular motors. In a second mode, (B), the cytoneme is generated at a non-producing receiver cell such as in the wing disc of *Drosophila* [40] and connects to a producer cell, from which it either receives a bolus of the morphogen Wg and then retracts, or receives multiple doses that are transported along the outside of the cytoneme (see (B)). We call this receiver-initiated transport (RIT). Finally, in a third type (C), both receiver and sender send out cytonemes that can create synapse-like connections to transfer morphogen from producer to receiver. This occurs in the chick limb bud, as shown in (C). In all cases, individual cells can employ multiple cytonemes. One sees that PIT is more direct since the receiver gets the signal upon contact with the cytoneme, whereas in the RIT mode the receiver must extend and retract the cytoneme to obtain the signal. Why Wnt transport in vertebrates uses the former whereas Wg transport in invertebrates is via the latter remains an open question.

One of the first experimental studies of the role of cytonemes showed how air sac primordia in the *Drosophila* wing disc extend cytonemes to both Fgf- and Dpp-secreting cells [33]. Recent work shows that they play a role in a wide variety of systems, including development of neuron types in the mouse neural tube [17] and in Hh transport in the wing disc [4]. At present the available experimental information is relatively high-level, demonstrating the existence of cytonemes and what their cargo is, but details on what

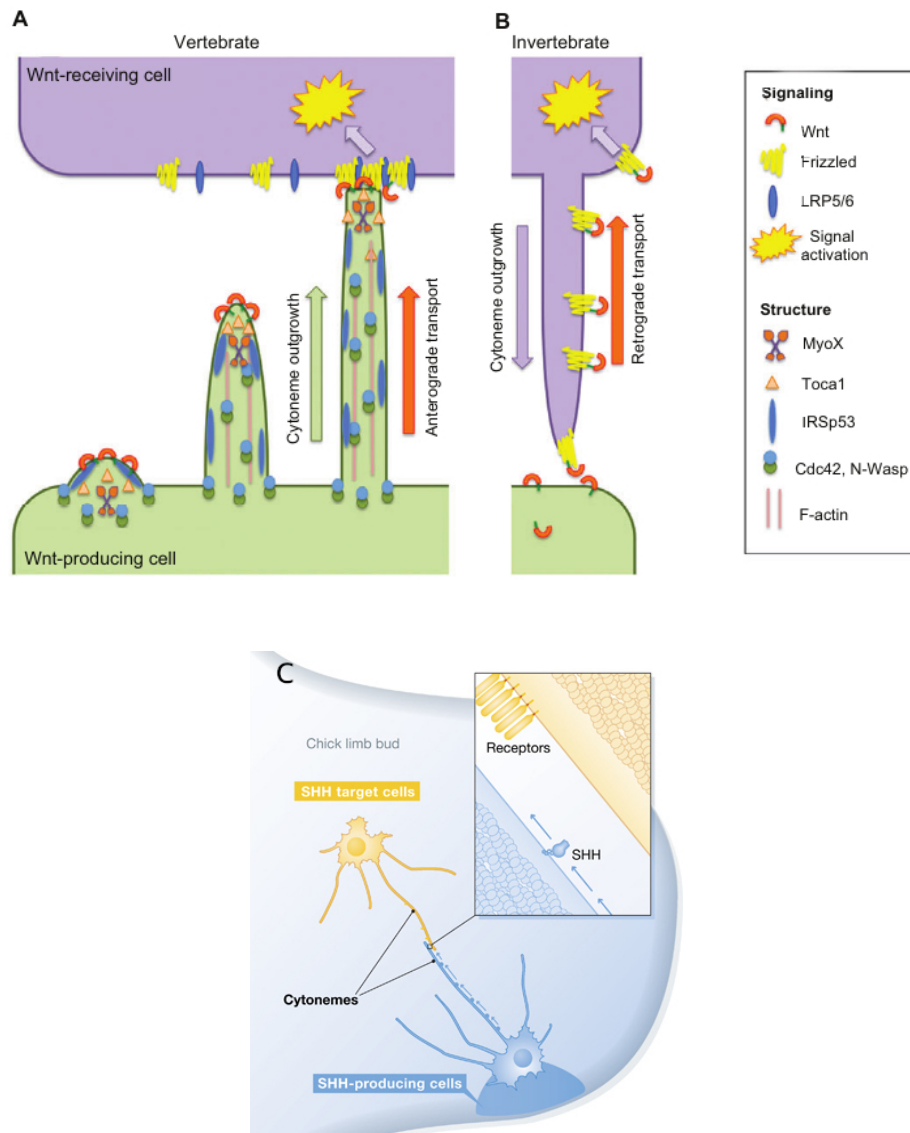


Fig 1. The three modes of cytoneme transport. (A) the PIT mode, (B) the RIT mode, (C) the synapse mode. Note that individual cells can give rise to multiple cytonemes. From [40] [(A) and (B)], and [24] (C).

controls the origination and number of cytonemes per cell in either the PIT or RIT mode remain sparse. Do extracellular signals bias the search process, or is the process random? How do cytonemes remain in contact during either loading or unloading of their cargo, and when vesicles are involved in PIT cytonemes, what determines when the transfer process stops? A number of recent reviews cover the variety of systems in which cytonemes play a role [10, 23, 37, 41, 49], but much remains to characterize the details of the processes involved.

Nonetheless, a number of models of communication and pattern formation based on cytonemes have been formulated. One of the first is that due to Vasilopoulos and Painter [46], in which the authors develop and analyze a model for fixed direct contacts between signaling and receiving cells. Their focus was on the effect of long-range signaling in lateral-inhibition mechanisms of the type used in Notch-Delta signaling, and in their model the signaling network is static and a weight function is used to define who gives what and who gets what. They show that a variety of new pattern types can be generated, including sparse patterns of isolated cells and large clusters or stripes. Other models have been based on static or dynamic extension or retraction of cytonemes and the resulting search process. Similar models in which cytonemes are

permanently attached to cells were analyzed in [43], wherein N cytonemes were statically-attached to cells in a one-dimensional array, and a deterministic rate of transport was determined by the distance from the source cell. The authors showed how this could lead to a spatial gradient in the array. Stochastic transport of packets of morphogen were incorporated in [5, 22], in which the authors described transport by a velocity jump process widely used to describe the movement of cells and organisms [30, 20]. Reversal of the direction of packets was incorporated in the model, but since packets are carried along actin fibers by myosin motors [17], pauses are admissible, but reversals of direction are not. More recently this model was applied at the level of a single cytoneme, which can pause and reverse, in a two-dimensional array of target cells [6]. A similar model was used to compare the steady-state gradient of morphogen resulting from cytoneme transport with that resulting from diffusion [12], and a recent computational model was used to analyze morphogen gradient establishment using cytonemes [1].

As we show herein, cytoneme transport is simple and direct, even in complex tissues, whereas diffusive transport frequently involves intermediate steps such as binding or cell-to-cell transport (transcytosis). Our first objective is to develop a population-based PIT model for the cytonemes from which we can predict the length distribution of cytonemes as a function of space and time, given that each is initiated at a random time at the source, driven by a Poisson process, and makes contact for delivery at random lengths (and hence 'age'). Another is to compare the distribution of morphogen resulting from cytoneme transport with that which results from using a macroscopic diffusion equation whose coefficients are based on microscopic properties.

While we do not cover many possibilities in this article, our goal is to lay the groundwork for more detailed cytoneme modeling. Further, more detailed modeling is also difficult because there is currently a dearth of experimental evidence, to understand how hypothetical interactions occur. We believe that the stochastic approach will be promising in the future because it is very flexible with regards to what can be added or removed from the model. In particular, the stochastic model we will introduce is discrete at the level of individual cytonemes and cells, and thus can easily incorporate additional effects and interactions as experimental evidence accrues towards understanding the behavior of cytonemes.

2 Cytoneme-based transport

We first consider several simple models to show how cytonemes spreading from a single cell can lead to a graded morphogen distribution. We will assume a constant cytoneme velocity, and later allow for pausing and other biologically-relevant processes.

2.1 Producer-initiated transport

We assume that there is a producer cell located at $x = 0$ that intermittently produces cytonemes at rate λ in a one-dimensional domain. The cytonemes extend at velocity v until they contact a receiver cell at some position x , and release their cargo instantaneously. The evolution of this system is governed by

$$\begin{aligned} \frac{\partial}{\partial t} p(x, t) + \frac{\partial}{\partial x} (v(x)p(x, t)) &= -\mu p(x, t) \\ \frac{\partial}{\partial t} M(x, t) &= \gamma \mu p(x, t) \end{aligned} \tag{1}$$

where $p(x, t)$ is the number density of cytoneme tips per unit length and μ is the cytoneme attachment rate at x . In the second equation, M is the amount of morphogen delivered per unit length, measured for example in molecules per unit of cell length, and γ is a conversion factor for the amount of morphogen delivered per cytoneme tip. We are implicitly assuming that each cytoneme carries the same amount of cargo and that every attachment is successful in delivering morphogen. We impose a boundary condition at $x = 0$ of the form $p(0, t) = \lambda(t)$, where λ is the number of new cytonemes produced as a function of time. If this equation refers to the position of a single cytoneme starting at $t = 0$, then $\lambda(t) = \delta(t)$. On other hand, if there is a probability distribution for the emergence of cytonemes, then $\lambda(t)$ is equal to the rate of that distribution.

The solution of the first equation can be found via the method of characteristics by setting

$$\begin{aligned} \frac{dt}{ds} &= 1 & t(\xi, 0) &= \xi \\ \frac{dx}{ds} &= v & x(\xi, 0) &= 0 \\ \frac{dp}{ds} &= -\mu p & p(\xi, 0) &= \lambda(\xi), \end{aligned} \quad (2)$$

where $s \geq 0$ parameterizes a characteristic and ξ parameterizes the curve $x = 0$. One finds that the solution is

$$p(x, t) = \lambda(t)H\left(t - \frac{x}{v}\right) e^{-\frac{\mu}{v}x}.$$

where H is the Heaviside function. While this model is very simple, it is already clear that an important factor in the morphogen distribution is the ratio μ/v , which essentially governs how quickly cytonemes halt compared with their extensional velocity. If this quantity is large, the steady-state morphogen distribution is highly concentrated at $x = 0$, whereas it is widely-distributed when it is small. The dynamic approach to the exponential distribution in space behind the front $x = vt$ is governed solely by the velocity - more rapid spreading occurs with a larger velocity - as is expected.

The distribution of morphogen received by the cells is then given by

$$M(x, t) = \gamma \int_0^t \mu p(x, \tau) d\tau = \gamma \mu e^{-\frac{\mu}{v}x} \int_{x/v}^t \lambda(z) dz$$

For $\lambda(t) = \lambda_0 H(t)$ where $H(t)$ is the heaviside function, the result is

$$M(x, t) = \gamma \mu \lambda_0 H\left(t - \frac{x}{v}\right) e^{-\frac{\mu}{v}x} \left(t - \frac{x}{v}\right)$$

Noteworthy is the fact that there is a time-delay after startup during which $M(x, t)$ is zero. This is in contrast to diffusive mechanisms, which instantaneously generate nonzero concentrations globally. Also note that for each x , once $t > x/v$, the concentration increases linearly in time at that point, with a coefficient dependent on x . These results are shown in Figure 2.¹

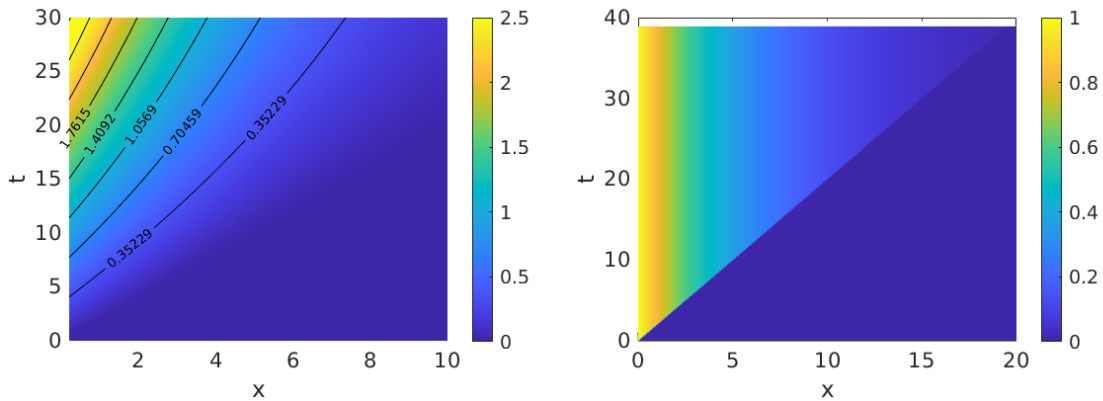


Fig 2. The morphogen concentration $M(x, t)$ as a function of x and t (left) and $p(x, t)$ (right) for the PIT model. The parameter values used are $\mu_d = 0.1$, $v = 0.5$ and $\lambda = 1$.

While there are many more details that can be analyzed for the PIT process, we next consider the RIT process in greater detail.

¹In this and the following figures we use dimensionless variables based on a time scale of 10 seconds and a length scale of 10 microns.

2.2 Receiver-initiated transport

Under RIT non-producers search for producers to extract a bolus of morphogen. This mode is interesting because the cargo has direct access to the cytosol, whereas in PIT the transfer is thought to involve surface receptors. Thus there may be local loss of signals if the bolus saturates the available receptors. When the cargo in RIT is a morphogen, it may bind to receptors in the cytosol to activate downstream signaling.

Suppose that when a cytoneme makes contact with a producer cell it loads its cargo, which could be a morphogen in a vesicle, and retracts. The cytoneme extension process can be modeled as above, except that the position of the receiver cell is now very important, and the stopping rate μ must now be spatially variable since cytonemes that stop and perhaps retract prior to reaching any producing cells would be ineffective. In particular, we fix the receiver cell at position $x_0 > 0$ and assume that the producer cells are located at $x = 0$. We further assume that attachment occurs instantaneously once a cytoneme reaches $x = 0$. Then the number density per unit length of extending cytoneme tips is governed by

$$\begin{aligned} \frac{\partial p_e}{\partial t} - v \frac{\partial p_e}{\partial x} &= 0, \quad x \in (0, x_0] \\ p_e(x_0, t) &= \lambda(x_0, t) \end{aligned} \quad (3)$$

where $\lambda(x_0, t)$ is the number density of cytonemes generated by the receiver cell.²

The number of cytonemes per unit of time that reach producer cells at $x = 0$ is $J(t) = v p_e(0, t)$, and the number of attached cytonemes, P_a evolves according to

$$\frac{dP_a}{dt} = J(t) - \mu_d P_a, \quad (4)$$

where μ_d is the detachment rate. After detachment, the cytoneme is presumed to be carrying a morphogen packet, and the density of cytoneme tip positions p_r for cytonemes laden with morphogen is governed by³

$$\begin{aligned} \frac{\partial p_r}{\partial t} + v \frac{\partial p_r}{\partial x} &= 0, \quad x \in [0, x_0) \\ v p_r(0, t) &= \mu_d P_a. \end{aligned} \quad (5)$$

This system can be solved analytically once $\lambda(x_0, t)$ is specified. In particular, let us assume that a cell turns on a constant rate λ_0 of cytoneme generation at $t = 0$, thus $\lambda(x_0, t) = \lambda_0 H(t)$ where $H(t)$ is the Heaviside step function. The solution is then

$$\begin{aligned} p_e(x, t) &= \lambda_0 H\left(t - \frac{x_0 - x}{v}\right) \\ P_a(t) &= \frac{\lambda_0 v}{\mu_d} H\left(t - \frac{x_0}{v}\right) \left(1 - e^{-\mu_d \left(t - \frac{x_0}{v}\right)}\right) \\ p_r(x, t) &= \lambda_0 H\left(t - \frac{x_0 + x}{v}\right) \left(1 - e^{-\mu_d \left(t - \frac{x_0 + x}{v}\right)}\right) \\ M(t, x_0) &= \gamma v \lambda_0 H\left(t - \frac{2x_0}{v}\right) \left[t - \frac{2x_0}{v} + \frac{1}{\mu_d} \left(1 - e^{-\mu_d \left(t - \frac{2x_0}{v}\right)}\right)\right] \end{aligned} \quad (6)$$

²In proposing this form of equation, we implicitly assume several things. Firstly, we assume that only the cytoneme tip contains morphogen. Thus we only need to track the tip position rather than the entire shape of the cytoneme. In addition, we assume that space-exclusion effects are negligible, which allows us to assume that each cytoneme moves independently of the others. The rationale behind these assumptions is that the cytonemes are quite small, and thus, even if there were many cytonemes in a small area, there would still be sufficient space for the cytonemes to wriggle through without strong interaction effects. On the other hand, it is important to note that there is a dearth of biological evidence for how cytonemes actually move through a tissue and whether they interact with one another or not. An example of interaction is shown in Figure 1(c), but this is between two different types of cytonemes. The effect of interactions between like types remains for future work, and will also hinge upon future experimental observations. It should also be noted that we do not track cytonemes that do not reach $x = 0$ since they do not contribute to the morphogen flux. To account for them one could include a 'death' term, but we ignore this.

³If there is a probability of an attached cytoneme failing to obtain a morphogen packet, we can scale the boundary condition on p_e by the probability of success to obtain the population of morphogen-laden cytonemes.

As before, the constant γ gives the amount of morphogen transferred per cytoneme, and M is the morphogen received by a cell at x_0 .

Due to the finite velocity, we see that at there is an initial time interval $(0, 2x_0/v)$ during which no morphogen is received, followed by gradual morphogen reception that depends on the attachment waiting-time distribution, and this gradually ramps up to a linear rate of increase with slope $v\gamma\lambda_0$. Note that this linear increase rate is independent of x_0 , but that the time-delay required to reach that rate is x_0 -dependent.

If there are many cells, each at different points, x_0 , then the overall cytoneme tip distribution can be found by considering the distributions (p_e , P_a and p_r above) as functions of x_0 and summing over x_0 . The concentration of morphogen in receiver cells will then increase in a wave-like fashion across the tissue due to the variable time-delays. However, if all cells have the same λ_0 and v , the concentration will approach a linearly decreasing function of x_0 after the exponential terms relax. This is in contrast to diffusion with decay, where the profile develops into an exponential.

However, this model is too simplistic, because cytonemes do not simply extend for indefinite lengths of time at a particular velocity, but are known to exhibit stopping and starting. In fact, the time spent resting is known to exhibit Poissonian statistics. Furthermore, some cytonemes may fail to reach their target and retract prior to receiving a morphogen packet. To account for these effects, we include decay terms and first-order reaction terms in the cytoneme extension and retraction equations, and introduce ordinary differential equations to describe the population of cytonemes in a resting phase. This leads to the following system,

$$\begin{aligned}
\frac{\partial p_e}{\partial t} - v \frac{\partial p_e}{\partial x} &= -\lambda_r p_e + \lambda_m r_1 - k_d p_e, & p_e(x_0, t) &= \lambda(t), & \text{extension} \\
\frac{dr_1}{dt} &= \lambda_r p_e - \lambda_m r_1, & & & \text{rest phase} \\
\frac{dP_a}{dt} &= v p_e(0, t) - \mu_d P_a, & & & \text{attachment} \\
\frac{\partial p_r}{\partial t} + v \frac{\partial p_r}{\partial x} &= -\lambda_r p_r + \lambda_m r_2, & v p_r(0, t) &= \mu_d P_a, & \text{retraction} \\
\frac{dr_2}{dt} &= \lambda_r p_r - \lambda_m r_2, & & & \text{rest phase} \\
\frac{dM}{dt} &= \gamma v p_r(x_0, t), & & & \text{morphogen accumulation}
\end{aligned} \tag{7}$$

where again, the domain is $(0, x_0)$. Here r_1 and r_2 are two distinct resting phases for the extending and retracting cytonemes. It is a minor technical complication that these two populations must be tracked separately, because otherwise we would lose track of which cytonemes in the resting phase contain morphogen and which do not. Note that the cytonemes that reverse prior to reaching the source region are not included in p_r since they do not contribute to the morphogen flux, but rather are simply eliminated via the degradation term $k_d p_e$.

The resulting system can be solved via Laplace transform, but the inversion integral appears to be non-elementary. Thus, we have solved the above system numerically using an upwind finite difference approximation to obtain results for $M(t)$ and the other quantities of interest. In comparison with the simpler model, the main additional quantities to study here are the decay rate k_d of cytonemes that fail to obtain morphogen, and the rates of state changes between resting and mobile states. The spatial distributions of the cytonemes for a cell fixed at $x_0 = 20$ are shown in Figure 3.

In that figure the value of $p(x, t) = p_e(x, t) + r_1(x, t)$ (the density of cytonemes in $(x, x + dx)$ at t) becomes larger when the average length of the resting phase increases. This is because as the average resting time increases, the cytoneme transport process is less efficient, and thus the time-average velocity of cytonemes decreases. At the same time, the cytoneme generation rate is not affected by the resting phase in our model, and thus on average, the same number of cytonemes are still generated in each time interval. Since cytonemes are not traveling as quickly, but are still generated at the same rate, the spatial density of cytonemes must then be higher in the absence of degradation. Also note that the profiles of extending and

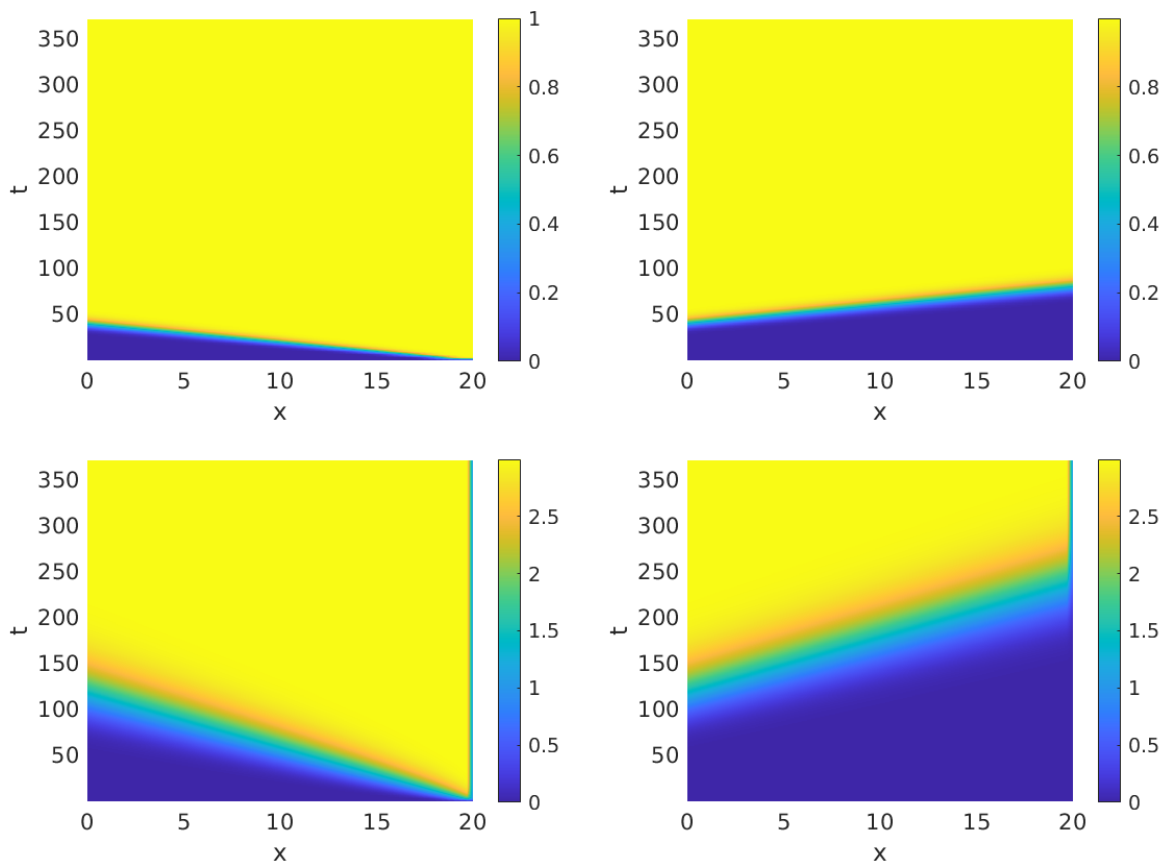


Fig 3. Plots of the space-time cytoneme tip location distribution – computed from Equation 6 – for cytonemes emanating from a cell at $x_0 = 20$. The top row is the pure advection case ($\lambda_r = 0$), with p_e on the left and p_r on the right. The bottom row includes a rest phase, with $p_e(x, t) + r_1(x, t)$ on the left and $p_r(x, t) + r_2(x, t)$ on the right. We set $\mu_d = 1s^{-1}$, $\lambda_m = 0.25s^{-1}$, $\lambda_r = 0.5s^{-1}$, and $v = 1\mu m/s$.

retreating cytonemes are qualitatively-inverted, as expected. With degradation, the degradation rate also figures into the balance, with a higher degradation rate leading to lower cytoneme densities.

Since the resting phase decreases the efficiency of cytoneme transport, one sees that although the number of cytonemes that exist simultaneously may be much larger than when there is no rest phase, the amount of morphogen delivered is largest when there is no resting phase. This leads to the question of why cytonemes exhibit a resting phase at all - it seems to only hinder the morphogen delivery process. While it is difficult to say precisely why cytonemes have resting phases, it may be that without biological regulation, the resting phases may be much longer than those observed, and that in fact, cytoneme transport processes have been fine-tuned to minimize the resting phase. Another aspect may be that working in one spatial dimension, the problem of orienting the cytoneme is not as significant as it would be for a cytoneme extending in a 3D or 2D tissue. It may be that during the resting phases, the cytoneme is integrating various guiding queues to ensure that it travels towards its target. Extending the model to include various aspects of cytoneme transport is an area of future interest, though we do make some initial inroads into the importance of cytoneme transport direction in the stochastic model described in the next section.

Before delving into a stochastic model, we conclude this section by describing several extensions that can be easily-included in the continuum model. In the models described above, we have conditioned on the receiver cell being located at some point, x_0 . However, it is straightforward to allow various starting points and then compute $M(t, x_0)$ to obtain the spatiotemporal dependence of the morphogen concentration in the receiver cells.

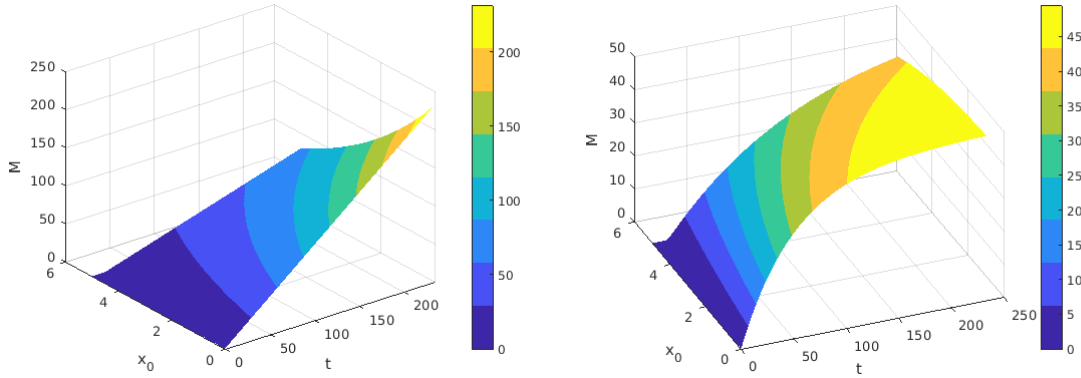


Fig 4. The evolving number of morphogen packets $M(t)$ received as a function of time and space. On the left there is no cellular feedback, so the cells continue receiving morphogen, whereas on the right, there is feedback that shuts off cytoneme generation after 50 packets are received. The bright yellow shows where M reaches its maximum, and one can see that this peak gradually expands outwards towards more distant cells as time progresses.

Secondly, when there is cytoneme degradation, the resulting concentration profile exhibits exponential decay rather than linear decrease. To understand this, one can think of the cytoneme extension process as a discrete random walk problem in which the cytoneme can either move forward or permanently stop at any time. Let α be the halting probability for a single step. Then, after n steps, the probability that a particular cytoneme has reached $x_n = n\delta x$ is $(1 - \alpha)^n$. Thus, if we consider a new cytoneme being added at each step at $x_0 = 0$, we find that after sufficient time, the probability of a cytoneme at x_k is $p(x_k) = (1 - \alpha)^k$. With $x_k = k/n$, and $\alpha_n = \alpha/n$, we hold k/n fixed and allow $n \rightarrow \infty$. In this limit, we obtain an exponential decay for the density of cytonemes in $(x, x + dx)$, because $\lim_{n \rightarrow \infty} (1 - \alpha_n)^{xn} = e^{-\alpha x}$.

Further details can be included if we allow receiver cells to alter the cytoneme production rate $p_e(x_0, t)$ in response to the amount of morphogen received. In this case the model becomes nonlinear, and cannot be solved analytically. Morphogen feedback might be expected biologically if we presume that the primary role of the morphogen is to activate some signalling cascade involved in cell differentiation. Once the appropriate level of the signal has been received, the cell would no longer require additional morphogen, and thus would not need to continue generating cytonemes. In this case, we set $\lambda(t) = \lambda(M(t))$ to be a decreasing function of M . In the simplest case, $\lambda = \lambda_0 - \lambda_1 q$ is a linearly decreasing function. The ratio λ_0/λ_1 determines the maximum amount of morphogen the cell will receive before it shuts off cytoneme generation. This leads to a wave of cells receiving a particular amount of morphogen, approximately $M = \lambda_0/\lambda_1$, as is shown in Figure 4.

Notice that since it takes distant receiver cells longer to reach the producers and return with morphogen, there is a lag between the morphogen concentration at more distant cells, and the morphogen concentration at the cells with x_0 near 0 (which is where the producer cells are located). Interestingly, if cells are able to shut off their cytoneme generation after sufficient morphogen has been received, and also only grow in response to adequate morphogen, this may yield a mechanism by which tissue size can be controlled.

2.3 Cytosome return rates and first-passage-time distributions

While the preceding results are based on a continuum description, assuming sufficiently-large population of cytonemes existing around each point in space and time to validate the continuum hypothesis, there is also a close connection between the previous models, and certain stochastic cytoneme models. In particular, let us assume that a single cytoneme undergoes alternating phases of extension (or retraction) and resting. The time intervals for each of these mobile or rest phases are presumed to be random variables that are Poisson-distributed with rates λ_m and λ_r . In other words, for a mobile phase, the probability that that

particular mobile phase exists for a time $T > t$ is

$$\mathbb{P}[T > t] = e^{-\lambda_m t}$$

and likewise for the rest phases with λ_m replaced by λ_r . Similarly, we have assumed that the attachment phase lasts for a Poisson distributed time with rate μ_d . One can show via the methods in [42] that with all of the distributions exponentially distributed, the resulting probabilities $p_e(x, t)$, $P_a(t)$, and $p_r(x, t)$ obey the same PDEs as in Equation (7), but with $k_d = 0$, and initial condition of the form $p_e(x, 0) = \delta(x - x_0)$ that describes the initial (deterministic) placement of the cytosome at $t = 0$. This is essentially a consequence of the fact that for i.i.d. random variables, the expectation of the mean is equal to the expectation of a single instance.

When considering just a single cytosome moving according to a stochastic process, a particularly important quantity is the distribution characterizing the time it takes for a cytosome to extend, upload some morphogen molecules or morphogen-containing vesicles, and return back to the receiver cell to deliver the morphogen. This probability distribution can be written as

$$\mathbb{P}[\text{return by } t \text{ after departing at } t_0 \text{ from } x_0] \equiv F(t|t_0, x_0) = \int_0^t f(t|x_0, t_0) dt$$

where $f(t|x_0, t_0)dt$ is the probability for a cytosome, originating at t_0 from a cell at x_0 returning back to the cell with morphogen in the interval $(t, t + dt)$. The return event is an example of a first-passage-time event. Thus, $F(t|t_0, x_0)$ represents the total probability that a cytosome has returned by time t , which is the cumulative distribution for the first-passage-time (FPT). FPT's have been applied to cytosome-mediated transport previously in [6], and we will consider several simple examples here.

First, recall Equations (6) where the extension (p_e), retraction (p_r), and attachment (P_a) probabilities were obtained for a cell generating cytosomes at a fixed rate starting at $t = 0$. If instead we condition the process on a cytosome being initiated at $t = 0$ in that example, we obtain

$$\begin{aligned} p_e(x, t) &= \delta\left(t - \frac{x_0 - x}{v}\right) \\ P_a(t) &= \frac{v}{\mu_d} H\left(t - \frac{x_0}{v}\right) e^{-\mu_d\left(t - \frac{x_0}{v}\right)} \\ p_r(x, t) &= H\left(t - \frac{x_0 + x}{v}\right) e^{-\mu_d\left(t - \frac{x_0}{v}\right)}. \end{aligned} \quad (8)$$

To compute the FPT distribution, we consider the fact that the probability of a cytosome passing the point $x = x_0$ in the interval $(t, t + dt)$ is equal to $vp_r(x_0, t)$, and that this is equivalent in the limit as $dt \rightarrow 0$ to the cytosome experiencing a first-passage event at t . Thus, we have that $f(t|x_0, t_0) = vp_r(x_0, t - t_0)$ for any $t > t_0$. The amount of morphogen received by the cell is then proportional to $F(t|x_0, t_0)$ which is just the integral of $f(t|x_0, t_0)$ from 0 to t .

As a slight modification, the FPT distributions may be allowed to be degenerate (integrate to some number $0 < \alpha < 1$) since some cytosomes may fail to ever upload morphogens, and simply return empty-handed. To see an example of how this may arise, consider a model where cytosomes extend at a velocity v as before, but have a probability β per unit time of halting and turning back regardless of whether it has reached the producer cells. Thus, the governing equations are those in Equations (3) through (5), but now we modify Equation (3) to become

$$\frac{\partial p_e}{\partial t} - v \frac{\partial p_e}{\partial x} = -\beta p_e$$

The solution, which again may be obtained via the method of characteristics, is

$$\begin{aligned}
 p_e(x, t) &= \delta\left(t - \frac{x_0 - x}{v}\right) e^{-\beta x/v} \\
 P_a(t) &= \frac{v}{\mu_d} H\left(t - \frac{x_0}{v}\right) e^{-\mu_d(t - \frac{x_0}{v}) - \beta x_0/v} \\
 p_r(x, t) &= H\left(t - \frac{x_0 + x}{v}\right) e^{-\mu_d(t - \frac{x_0}{v}) - \beta x_0/v}.
 \end{aligned} \tag{9}$$

The FPT density is as before, but now multiplied by a factor $\pi_0 = e^{-\beta x_0/v}$. This factor is called a splitting probability and we can thus write the FPT density as $\pi_0(x_0)f(t|x_0, t_0)$ where f is unitary.

We also consider a more complex example in which the cytonemes extend, but can rest for intermittent intervals of time. Thus, they alternate between motile phases and rest phases. As in [35], we assume that both the motile and resting phases obey Poisson distributions, albeit with different rates, denoted μ_m and μ_r . This stochastic process is an example of an alternating renewal process, and these have been analyzed in [36, 9, 6]. While non-trivial, the exact FPT for a cytoneme obeying this process is computable via Laplace-transform methods.

The first-passage-time distribution can be computed via similar techniques to those in [25, 6], and the details are given in the appendix. We find that

$$f(t|x_0) = \int_0^t \left[\mu_d e^{-\mu_d(t-\tau)} H\left(\tau - \frac{2x_0}{v}\right) \left[e^{-(\tau + \frac{x_0}{v})\lambda_m} \sqrt{\frac{c}{(\tau - \frac{2x_0}{v})}} I_1\left(2\sqrt{c\left(\tau - \frac{2x_0}{v}\right)}\right) + \delta\left(\tau - \frac{2x_0}{v}\right) \right] \right] d\tau$$

with $c = 2\lambda_m\lambda_r x_0/v$ and $I_1(z)$ is the modified Bessel-function of order 1. This distribution is quite complex, but the moments of the distribution can be found easily by differentiating the Laplace transformed FPT (which is comparatively simpler) to obtain

$$\langle t \rangle = \frac{1}{\mu_d} + \frac{2x_0}{v} \left(1 + \frac{\lambda_m}{\lambda_r}\right)$$

Notice that the two terms, $1/\mu_d$ and the velocity dependent term essentially account for 1) the time the cytoneme is attached to the producer cell, and 2) the time it takes to go out and come back.

The variance can be computed by taking the second derivative of the Laplace-transformed FPT at $s = 0$ and subtracting $\langle t \rangle^2$. This leads to

$$\sigma^2(t) = \langle (t - \langle t \rangle)^2 \rangle = \frac{1}{\mu_d^2} + \frac{4x_0}{v} \frac{\lambda_m}{\lambda_r^2}$$

which again, has components due to the variance of waiting while attached, and of the time it takes to travel to and from the producer cells. Note that in contrast to other models [6], the cytonemes do not have periods of forward and backward motion while extending. Rather, they have periods of forward motion with interspersed pauses with no motion. We believe this more realistically captures the dynamics of cytonemes which we expect exhibit highly biased transport towards a target. Nonetheless, the two models are similar, and setting $v_- = 0$ in [6] should yield results very similar to ours here.

3 Stochastic models of cytoneme-based transport

In the continuum models introduced thus far, each quantity refers to an average number of morphogen packets, but because individual cells only maintain a small number of cytonemes at any moment, it is important to consider other quantities such as the variance in the number of morphogen packets received during transport. This has further relevance since it appears that in many cases morphogen delivery is not a continuous process, but coincides with the arrival of discrete punctae, thought to be vesicles containing high levels of morphogen. This would be expected to produce bursts of morphogen at discrete times, separated by intervals where no new morphogen arrives. To understand such quantities, further details of the stochastic nature of the cytoneme generation and morphogen delivery must be taken into account, and we address this in this section.

3.1 Multiple cytonemes emanating from a receiver cell

We consider a single receiver cell located at x_0 that extends cytonemes to reach source cells located at $x = 0$ as above, but now we analyze the more realistic situation in which the cytoneme generation rate is stochastic. In general, a complete analysis is too complex, but some analytical results can be obtained if cytoneme generation follows a Poisson process, which implies that there is no correlation between the generation of one cytoneme, and the time at which a subsequent one is generated. Rather, there is simply a smoothly varying rate (or intensity) $\lambda(t)$ such that $\int_{t_1}^{t_2} \lambda(t) dt$ gives the expected number of new cytonemes generated in (t_1, t_2) . This description is relevant in reality since individual cells can support multiple cytonemes, and these cytonemes may form in different regions of the cell, thus removing correlations (or anti-correlations) between the times for subsequent cytonemes to be generated. The Poisson process approach also seems reasonable for describing the generation of cytonemes amongst an array of cells as long as cytoneme generation in a given cell does not significantly alter the cytoneme generation capabilities of its neighbors.

Thus let $X(t)$ be a Poisson process of rate λ , and let E_1, E_2, \dots, E_n be the events of generating cytonemes in $(0, T]$. We seek the joint distribution of the random times of the E_i conditioned on the event $N(T) = n$. The probability $P(N(T) = n)$ for a non-homogeneous Poisson process of intensity $\lambda(t)$ is given by

$$P(N(T) = n) \equiv p_n(T) = \frac{\left(\int_0^T \lambda(\tau) d\tau\right)^n}{n!} e^{-\int_0^T \lambda(\tau) d\tau},$$

while for a time-homogeneous Poisson process λ is constant, and

$$p_n(T) = \frac{(\lambda T)^n}{n!} e^{-\lambda T}.$$

We can also compute quantities such as the expectation and variance of the cytoneme distributions as follows. For instance, let $x(t|t_i)$ be the position at time t of a cytoneme tip that originated at the event time t_i . If the cytoneme transport is simply advective, then this is equal to $x_0 - v(t - t_i)_+$ where $u_+ = \max(0, u)$. Then, since $\{t_i\}$ is IID, given a fixed number $N(t) = n$ of cytonemes the expectation of the average position is simply the expected position of any individual cytoneme⁴

$$\mathbb{E}_n \left[\frac{1}{n} \sum_{i=1}^n x(t|t_i) \right] = \mathbb{E}_1[x(t|\tau)] = x_0 - \frac{vt}{2}.$$

Since this result is independent of n , it also gives the mean position when N is allowed to be a random variable. More generally, for some quantity $Q(t|t_i)$ that depends only on a single t_i from an IID set, the expectation of the average over any point process is simply the expectation of $Q(t|\tau)$,

$$\mathbb{E} \left[\frac{1}{N(t)} \sum_{i=1}^{N(t)} Q(t|t_i) \right] = \mathbb{E}_1[Q(t|\tau)]. \quad (10)$$

On the other hand, the expectation of the sum $\sum_{i=1}^{N(t)} Q(t|t_i)$ is

$$\mathbb{E} \left[\sum_{i=1}^{N(t)} Q(t|t_i) \right] = \mathbb{E}[N(t)] \mathbb{E}_1[Q(t|\tau)] = (\lambda t) \mathbb{E}_1[Q(t|\tau)]. \quad (11)$$

Higher order moments such as the variance can be found as follows. We write

$$\sigma^2 \left(\frac{1}{N(t)} \sum_{i=1}^{N(t)} x(t|t_i) \right) = \sum_{n=0}^{\infty} p_n(t) \mathbb{E}_n \left[\left(\frac{1}{n} \sum_{i=1}^n x(t|t_i) - \mathbb{E}_1[x(t|\cdot)] \right)^2 \right]$$

⁴We use the notation $\mathbb{E}_n[\cdot]$ to indicate expectations that are conditional on $N(t) = n$

To evaluate this we split the squared-sum in the formula above into a sum of diagonal terms $i = j$ and an 'off-diagonal' term with $i \neq j$. After simplification, this yields⁵,

$$\begin{aligned}\sigma^2(x) &= \sum_{n=0}^{\infty} \frac{(\lambda t)^n}{n!} e^{-\lambda t} \left[\frac{1}{n} \mathbb{E}_1(x(t|\tau)^2) + \frac{n-1}{n} (\mathbb{E}_1 x(t|\tau))^2 \right] - \left(x_0 - \frac{vt}{2} \right)^2 \\ &= \sum_{n=0}^{\infty} \frac{(\lambda t)^n}{n!} e^{-\lambda t} \frac{1}{n} \sigma_1^2(x(t|\tau)) = \frac{(vt)^2}{12} e^{-\lambda t} \int_0^{\lambda t} \frac{1 - e^{-z}}{z} dz.\end{aligned}\quad (12)$$

Note that the x_0 terms all drop out of this expression. This is due to the fact that x_0 is fixed in this calculation, and thus the variance in the cytoneme position is independent of x_0 .

More generally, $Q(t|t_i)$ could be more complicated, such as the probability of the cytoneme having returned to the starting point or reached the source cells. Under the above conditions the variance of the average or the total sum of $Q(t|\cdot)$, given by

$$\sigma^2 \left(\frac{1}{N(t)} \sum_{i=1}^{N(t)} Q(t|t_i) \right) \quad \text{or} \quad \sigma^2 \left(\sum_{i=1}^{N(t)} Q(t|t_i) \right)$$

can then be computed. For the mean, $\frac{1}{N(t)} \sum Q(t|t_i)$, the variance of the mean is found by generalizing Equation (12) as follows

$$\sigma^2 \left(\frac{1}{N(t)} \sum_{i=1}^{N(t)} Q(t|t_i) \right) = \sigma_1^2(Q(t|\tau)) e^{-\lambda t} \int_0^{\lambda t} \frac{1 - e^{-z}}{z} dz \quad (13)$$

where

$$\sigma_1^2(Q(t|\tau)) = \int_0^t Q^2(t|\tau) \rho_1(\tau) d\tau - \left(\int_0^t Q(t|\tau) \rho_1(\tau) d\tau \right)^2.$$

For the sum, the result is an example of the law of total variance

$$\sigma^2 \left(\sum_{i=1}^{N(t)} Q(t|t_i) \right) = \mathbb{E} \left(\sigma_N^2 \left(\sum_{i=1}^N Q(t|t_i) \right) \right) + \sigma^2 \left(\mathbb{E}_N \left(\sum_{i=1}^N Q(t|t_i) \right) \right)$$

where the outer expectation and variance are with respect to $N(t)$ being arbitrary, and the inner terms are conditional on $N(t) = n$. Thus,

$$\sigma^2 \left(\sum_{i=1}^{N(t)} Q(t|t_i) \right) = \sum_{n=0}^{\infty} p_n(t) \left(\mathbb{E}_n \left(\sum_{i=1}^n Q(t|t_i) - n\mu \right)^2 + (n - (\lambda t))^2 \mu^2 \right)$$

where $\mu = \mathbb{E}_1[Q(t|\tau)]$. After simplification, this yields,

$$\sigma^2 \left(\sum_{i=1}^{N(t)} Q(t|t_i) \right) = (\lambda t) \mathbb{E}_1[Q(t|\tau)^2] \quad (14)$$

Thus, for a Poisson process, the mean and variance can be computed in a straightforward manner even when Q is very complicated.

⁵To see the last simplification below, recall that $\sum_{n=0}^{\infty} \frac{z^n}{n!} = e^z$, and that the integral $\int z^n dz = \frac{1}{n+1} z^{n+1}$. Thus, formally, we can consider $\sum_{n=1}^{\infty} \frac{1}{n} \frac{z^n}{n!} = \int \sum_{n=1}^{\infty} \frac{z^{n-1}}{n!} dz = \int \frac{e^z - 1}{z} dz$. The resulting exponential integral is a transcendental function and cannot be further reduced into a finite combination of other elementary functions.

3.2 Composite random processes

In the foregoing the secondary variable $x(t|t_i)$ is deterministic when t_i is fixed, but this can be generalized as follows. If the analog of the position is a Bernoulli random variable $R(t|\tau)$, for example $R = 1$ if a cytoneme has returned to x_0 and 0 otherwise, then the mean and variance of R are equivalent. In this case, it is also possible to compute the distribution function,

$$S(N_r, t) \equiv \mathbb{P} \left[\sum_{i=1}^{N(t)} R(t|t_i) - N_r \geq 0 \right] = \sum_{n=0}^{\infty} p_n(t) \mathbb{P}_n \left[\sum_{i=1}^n R(t|t_i) > N_r \right] \quad (15)$$

where \mathbb{P}_n indicates a conditional probability given $N(t) = n$. We define $\bar{r}(t) = \mathbb{E}_1[(r(t|\cdot))]$ as the probability for an individual cytoneme to have returned by time t when it could have started at any $\tau \in (0, t)$. The computation of the resulting distribution has been derived in [36] and an alternate derivation is presented in the appendix. The result is that the overall expectation is exponentially distributed with

$$S(N_r, t) = 1 - e^{-\lambda t \bar{r}(t)} \sum_{j=0}^{N_r-1} \frac{(\lambda t \bar{r}(t))^j}{j!}$$

Furthermore, if N_r is a fixed number, then by writing

$$\mathbb{P} \left[\sum_{i=1}^{N(t)} R_i = N_r \right] = S(N_r, t) - S(N_r + 1, t) = \frac{1}{N_r!} e^{-\lambda t \bar{r}(t)} (\lambda t \bar{r}(t))^{N_r},$$

we see that the resulting distribution for the number of packets received is Poisson-distributed with parameter $\lambda t \bar{r}(t)$, which is the product of the probability of a cytoneme returning with morphogen, times the expected number of cytonemes generated in $(0, t)$. Thus, the mean and variance of the number of packets received are $\lambda t \bar{r}(t)$ which depends on the FPT for a cytoneme to return to the cell with a packet of morphogen. Note also that as t increases, $\bar{r}(t)$ increases and eventually approaches a number $0 < \alpha < 1$ which is the probability of a cytoneme returning to a cell with morphogen at any t . Thus, in the long term, the number of cytonemes that bring morphogen to a cell approaches $\alpha \lambda t$ with λt representing cytoneme generation, and α an efficiency factor that describes how likely they are to find their target.

These results are also particularly interesting since the dynamics of the cytoneme extension, adhesion, and retraction processes are all summarized in $r(t|\tau)$ (even if $r(t|\tau)$ is for instance the complicated FPT from the previous section), but regardless of how complex $r(t|\tau)$ is, if the cytoneme generation is a Poisson process, then the morphogen received will be exponentially distributed with a parameter that depends on the cytoneme dynamics.

So far, we have assumed that variations in the amount of morphogen per cytoneme are not important. But, if there is a significant variation, a similar approach can be used, although a closed form is not possible in general as some of the simplifications used to obtain the results above no longer apply. If we wish to compute the distribution,

$$P(m, t) = \mathbb{P} \left[\sum_{i=1}^{N(t)} q(t|t_i) \geq m \right]$$

where $M(t|t_i)$ is the amount of morphogen returned to the cell by the cytoneme that was originated at t_i , then assuming that the amount of morphogen carried per cytoneme is independent of time and of any previous cytonemes, we obtain

$$P(m, t) = \sum_{n=0}^{\infty} p_n(t) \left[\sum_{j=0}^n \binom{n}{j} \bar{r}(t)^j (1 - \bar{r}(t))^{n-j} \mathbb{P} \left[\sum_{i=1}^j M_i \geq m | j \right] \right]$$

where the conditional probability

$$\mathbb{P} \left[\sum_{i=1}^j M_i \geq m | j \right] = \int_m^{\infty} \mathcal{M}^{(j)}(m) dm$$

is conditioned on j -cytonemes returning to the cell by time t . The symbol $\mathcal{M}^{(j)}$ is the j -fold convolution of the distribution function for M_i . It does not appear that this sum can be simplified to obtain a closed-form for the distribution. On the other hand, we expect that cells only produce limited numbers of cytonemes, thus n need not be taken very large and it may be possible to numerically approximate the summation under biologically reasonable assumptions. We did not investigate this here since the distribution of morphogen per cytoneme is currently unknown, but we hope that this example displays the usefulness of the stochastic analysis, and may be soon compared with experimental results as they arise.

Finally, to conclude this section, we also mention that Equation (10) is particularly important since it connects the stochastic and continuum models by giving a definition for the average number $n(x, t)dx$ of cytoneme tips in a small interval, $(x, x + dx)$. Since the cytoneme velocity is fixed, this quantity is equal to the number of cytonemes generated in $t \in (x/v, (x + dx)/v)$, which is on average $\lambda dt H(t - x/v)$, as was found above.

If we allow $n(x, t)$ to be indexed as well by the starting position, x_0 of the cytoneme, then $n(x, t|x_0)$ is essentially $p_e(x, t|x_0)$ from the model given above. Let us then consider $q(t|x_0)$, and compute for a given x_0 the mean and variance of this quantity. Given the continuum model above, the mean is exactly that obtained from the continuum model. In particular, let us define $m(t|x_0, t_0)$ as the distribution of arrival times for a cytoneme starting from x_0 at time t_0 , then

$$q(t|x_0) = \int_0^t m(t|x_0, \tau) \lambda(\tau) d\tau = \gamma v \lambda_0 H\left(t - \frac{2x_0}{v}\right) \left[t - \frac{2x_0}{v} + \frac{1}{\mu_d} \left(1 - e^{-\mu_d(t - \frac{2x_0}{v})}\right) \right]$$

For the variance, we then have

$$\begin{aligned} \sigma^2(m(t|x_0)) &= \int_0^t m^2(t|x_0, \tau) \lambda(\tau) d\tau \\ &= \int_{2x_0/v}^t \left[\frac{\gamma v}{\mu_d} \left(1 - e^{-\mu_d(t - \frac{2x_0}{v})}\right) \right]^2 \lambda_0 d\tau \\ &= \frac{\lambda}{\mu_d} \left(tv - 2x_0 - \frac{v}{\mu_d} \left(3 + e^{-2\mu_d t + \frac{4\mu_d x_0}{v}} - 4e^{-\mu_d t + \frac{2\mu_d x_0}{v}}\right) \right) H\left(t - \frac{2x_0}{v}\right) \end{aligned}$$

A similar analysis is valid if we allow a spatial Poisson process to describe generation between multiple cells at various starting points, x_0 . In that case, we introduce a spatial number density $\mu^{(1)}(x)$ which is defined such that for any set $B \subset \mathbb{R}^n$, we have

$$\mathbb{E}[N(B)] = \int_B \mu^{(1)}(x) dx.$$

We can also define similar conditional densities on subsets, B , e.g. $\nu_B^{(1)} = \mu^{(1)}(x) / \int_B \mu^{(1)} dx$. Let us assume that the spatial and temporal components are decoupled, e.g. the density $\rho^{(n)}((x_1, t_1), \dots, (x_n, t_n)) = \rho^{(n)}(t_1, \dots, t_n) \nu^{(n)}(x_1, \dots, x_n) = \prod_{i=1}^n \rho^{(1)}(t_i) \nu^{(1)}(x_i)$. Likewise, we obtain the mean,

$$\mathbb{E} \left[\sum_{i=1}^n r(t_i, x_i) \right] = \lambda \mu \int_{\Omega} \int_0^t r(\tau, x) d\tau dx$$

which is analogous to the mean computed above, except that we must now integrate over space as well as time. The variance follows this same trend. While statistics of this compound stochastic process can be computed analytically in these simple cases where all of the processes are independent of one another, it is clearly of scientific interest to incorporate interactions between competing processes as well. While perturbation expansions of the above results may be feasible for weak interactions, strong interactions require an alternative approach since it is not valid *a priori* to assume that strong interactions can be modeled via a series expansion with respect to a non-interacting system. Thus, we next develop a stochastic simulation algorithm that can deal with general interactions.

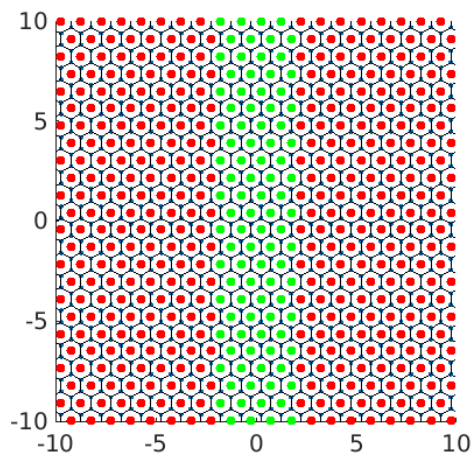


Fig 5. The underlying grid for the problem. Cells marked in green are producer cells, all other cells are receivers.

3.3 Stochastic simulations

As shown above, analytical results can be obtained when the cytoneme models obey certain assumptions so that the equations are workable. However, with an eye towards more complex models, for instance, where there are interactions between cytonemes, or when there is additional signalling occurring, we developed a stochastic simulation algorithm that considers the dynamics and internal states of each individual cytoneme to study cytoneme-based morphogen transport. We first consider the RIT problem, and to begin we lay down a hexagonal array of cells, with a stripe of morphogen producing cells located near the y -axis in the center of the domain and receiving cells located on either side of this strip (see Figure 5).

The following algorithm is used to update the temporal evolution of the cytoneme generation and cytoneme position processes in increments of length δt . The model parameters and typical values in dimensionless form are given in Table 1, and a diagram of the possible state changes is shown in Figure 6.

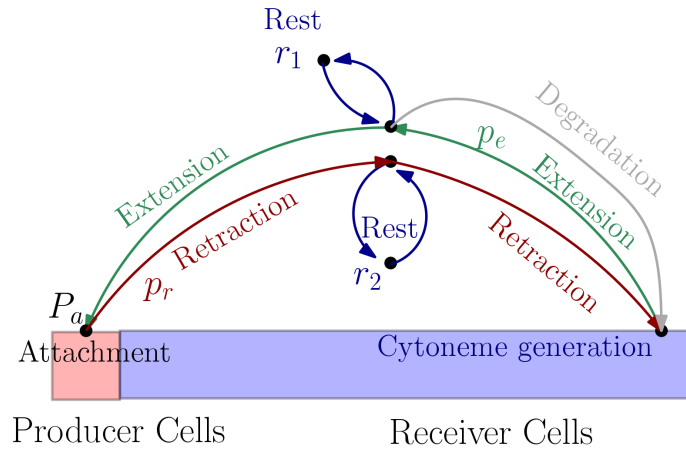


Fig 6. A diagram of the various transitions that can occur in the RIT model. Cytonemes start in the extension phase after generation. At any point, they may enter a rest state at a rate r_1 , or spontaneously begin retracting without reaching the source (degradation). If they reach the source, they become attached, and then undergo retraction, or enter intermittent rest phases at a rate r_2 as they retract.

1. Each receiver cell generates a new cytoneme with probability $p_i = 1 - e^{-\lambda\delta t}$
2. For all cells that generated a new cytoneme, the directional orientation of that cytoneme is chosen from a uniform distribution $\mathcal{U}(-\theta_0, \theta_0)$ so that the cytonemes can emanate from any cell in a cone-shaped region of angular width $2\theta_0$ opening towards the source cells.
3. For each cytoneme, the position is updated at each time step as $\mathbf{x}(t + \delta t) = \mathbf{x} - \delta t \mathbf{v}(\ell, \theta, t)$ where $\ell = |\mathbf{x}(t) - \mathbf{x}(t_0)|$ and t_0 is the time the cytoneme was initiated. The velocity could simply be a constant, or could be a function of direction, length and time.
4. For each cytoneme, there is also a probability $p_f = 1 - e^{-\lambda_r\delta t}$ that the cytoneme will go from extension to retraction at each time step.
5. When a cytoneme is located near a producing cell, there is an additional probability $p_a = 1 - e^{-\mu\delta t}$ of attaching to a producing cell and receiving a morphogen-packet. We assume that all morphogen packets carry equal amounts of morphogen at their origin, and thus the total amount each receiving cell gets is proportional to the number of packets it has received.
6. If a cytoneme is successful at obtaining a packet, then it switches to the retraction state, and its position is updated at each time step by $\mathbf{x}(t + \delta) = \mathbf{x}(t) - \mathbf{v}_r\delta t$
7. If a cytoneme length reaches $\ell = 0$, that cytoneme is eliminated. If that cytoneme was carrying a morphogen, one morphogen packet is added to the total received by the cell that originated the cytoneme.

This simple stochastic simulation approach is straightforward to implement and allows for simulations with thousands of producing and receiving cells that approach realistic scales that can be compared with biological tissues. A key result from a simulation is that we can in a straightforward manner obtain the distribution of morphogen, and of cytoneme lengths and positions throughout the tissue dynamically as the simulation evolves.

The morphogen distribution from a typical simulation is shown in Figure 7 to illustrate the typical output. At the top the source strip is the column of cells at the center and outside that each dot represents a single cell, colored according to the number of morphogen packets received. It is clear that the amount of morphogen received decays with distance from the source region,

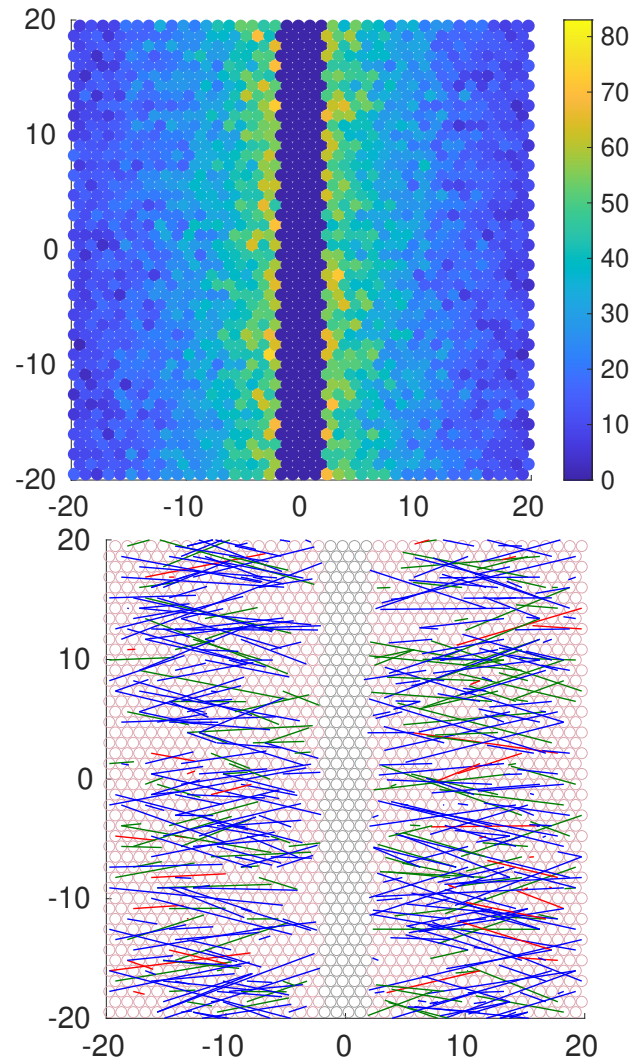


Fig 7. Depiction of the result of a typical simulation with 920 cells. (Top) Coloring corresponds to the number of morphogen packets received and the colorbar gives the number scale. The center column of cells are the source cells. (Bottom) Diagram of the cytonemes during a simulation at $t = -rcolx..$ Black cytonemes are extending, red are retracting without morphogen, and green received a morphogen packet and are retracting.

Symbol	Definition	Default Value
λ	Cytoneme generation rate	0.4
μ	Cytoneme attachment rate	100
v_0	cytoneme velocity	1
λ_r	cytoneme halting rate	1
θ	cytoneme angle	$-\pi/8 \leq \theta \leq \pi/8$
δt	time-step length	0.01

Table 1. Typical parameter values for the stochastic simulation method. Typical length scales are on the order of a μm , and time scales on the order of 1 second.

The spatial distribution of the cytonemes is shown in the bottom of Figure 7. In particular, cells close to the source can rapidly extend cytonemes, receive morphogen and retract, thus it appears at any point in time that there are less cytonemes emanating from the closest cells, even though they receive the most morphogen overall. Additionally, we see that more of the red retracting cytonemes (those that never reached a source cell) emanate from more distant cells, indicating that the likelihood for a successful morphogen transfer depends on distance from the producing cells, as expected.

Collapsing the morphogen distributions in Figure 7 to a one-dimensional distribution for each value of x leads to the distributions shown in Figure 8 for different parameters governing the morphogen generation rate, velocity parameters, and likelihood of receiving a morphogen packet. The main parameters that are varied there are the starting velocity of the cytoneme (v_0), the cytoneme halting rate (λ_r), and the attachment rate in the source region (μ). The following observations emerge from this. Increasing v_0 tends to yield flatter profiles of longer extent. Increasing λ_r leads to shorter morphogen distribution profiles, and much less morphogen transferred per unit time, and increasing μ only changes the distribution of the number of packets sent from cells within the source region. In particular, with high μ , only the source cells at the boundary of the source region will make many attachments, since the attachment dynamics are fast enough to make it unlikely that any cytonemes pass over the boundary to the interior. In most cases, we also see that the variance of the morphogen packets received scales with the mean number of morphogen packets received for cells located at position x .

Aside from the distribution of morphogen, it is also interesting to study the length distribution of cytonemes in the tissue. Understanding the length distribution may serve as a means to distinguish different transport processes that may yield similar morphogen profiles - for instance whether the transport is receiver- or producer-initiated. The cytoneme length distribution is obtained via a non-parametric kernel smoothing approach. The length of every currently existing cytoneme is computed at each step of the simulation, and we approximate the length distribution for that step as

$$p_b(t, \ell) = \sum_{k=0}^{N_c} k_b(\ell - \ell_k)$$

where b is a bandwidth parameter that governs how smooth the resulting approximate distribution is. In practice, the dynamics are quite noisy if this is simply computed at each time step. Thus, we also apply smoothing in the time-domain by summing over t for a range of values, e.g.

$$p_{b,m}(t, \ell) = \sum_{s=t-m\delta t}^{s=t+m\delta t} \sum_{k=0}^{N_c(s)} k_b(\ell - \ell_k)$$

The resulting distributions are shown as a function of time in Figure 9 for several different parameter ranges. Notice that as the velocity increases (from left to right), the distribution becomes less concentrated near $\ell = 0$, and hence a broader morphogen distribution, as expected. We also see that with a faster velocity, the 'steady-state' length distribution is achieved more rapidly.

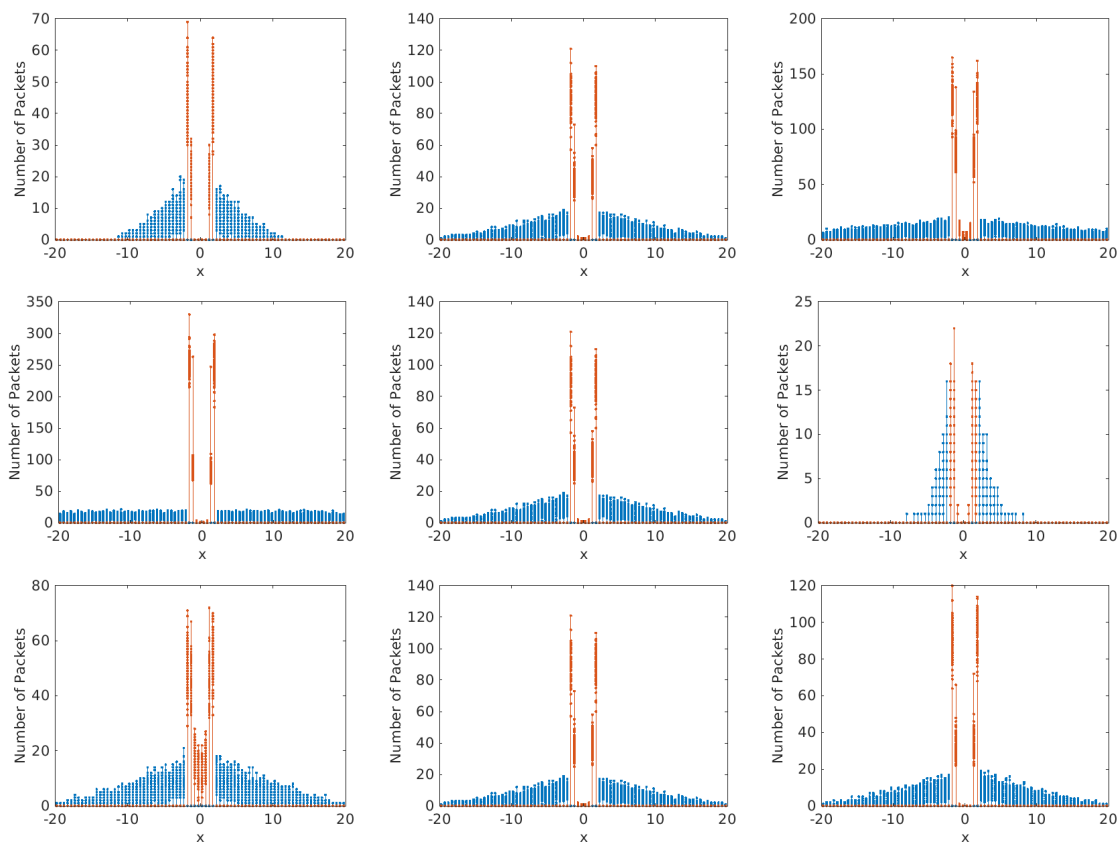


Fig 8. The spatial distribution of morphogen as a function of distance from the morphogen source under several different combinations of the parameters. In each row from right-to-left, one parameter is increasing. The top row has the initial cytoneme velocity, $v_0 \in \{0.5, 1, 2\}$. The middle row has the stopping rate for cytonemes in the range $\lambda_r = \{0.01, 0.1, 1\}$, and the bottom row has the attachment rate in the source region in the range $\mu = \{1, 5, 10\}$

3.4 Cell saturation effects

In the above results, the cytoneme generation dynamics and the cell morphogen accumulation are independent. For receiving cells, this means that the amount of morphogen received has no bearing on the cells rate of cytoneme generation, and for source cells, the number of packets transferred has no effect on their ability to transfer more packets as subsequent cytonemes attach. In reality, there can be limiting steps in each case.

Negative feedback loops are commonly found in morphogenetic systems. For receiving cells, this often leads to a control system where, as morphogen is received, the cell down-regulates the receptors for that morphogen. This could lead to saturation effects, and in a biological setting may have the purpose of modifying the morphogen distribution such that more distant cells can receive morphogen rather than all of it being absorbed by cells near the source. In our simulations, this effect can be implemented by modifying the cytoneme generation rate of cells as a function of the amount of morphogen they have received. This effect leads to a traveling front, where row-by-row, cells reach their saturation point leading to an expanding region of cells at nearly constant morphogen concentration. This is depicted in Figure 10, and described in more detail below.

When cells can shut-off their cytoneme machinery after receiving a certain level of morphogen, there is a significant dynamic behavior that differs from the previous case. Rather than attaining an equilibrium length distribution, and a morphogen distribution that simply scales with time, in this case there is a traveling-wave

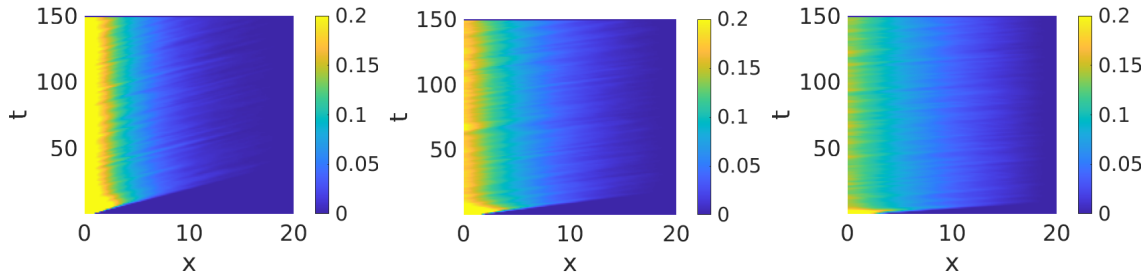


Fig 9. The cytoneme length distributions as functions of ℓ and t . On the left $v_0 = 0.5$ and $\mu_0 = 0.1$, in the middle $v_0 = 1$ and on the right $v_0 = 2$.

like propagation of cell-saturation. This starts with the closest receiver cells to the producer region which attain saturation morphogen levels rapidly followed by the gradual saturation of increasingly distant cells. Finally, the cytoneme production turns off once nearly all cells have achieved saturation.

To highlight this effect, the length and morphogen distribution are depicted as functions of time and length (position) showing how the evolution varies in 1) no saturation, 2) high morphogen saturation, and 3) low saturation. In the no-saturation case, the result is as before. In the high-saturation case, a large amount of morphogen is required to saturate a cell, so the results also appear fairly similar for a long time until eventual saturation is reached. In the low saturation case, only a small number of morphogen packets are needed to saturate a cell, and the behavior is distinctly different.

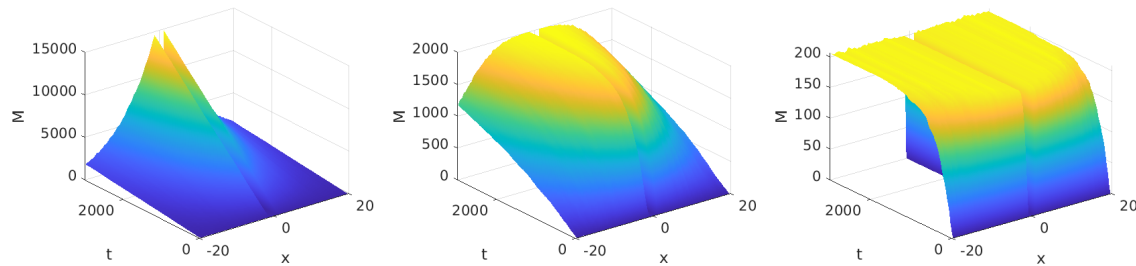


Fig 10. Depiction of the space-time dependence of the morphogen distribution. With increasing negative feedback, one can see that the concentration rapidly levels off. Feedback is increasing from left to right.

It is also interesting to consider what effect morphogen production dynamics play in the producing cells. The most direct approach appears to consider that morphogen packets are produced according to a stochastic process that has a saturation point, e.g.

$$\frac{d}{dt}P(M = m, t) = \lambda(m - 1)P(m - 1, t) - (F(t) + \lambda(m))P(m, t) + F(t)P(m + 1, t)$$

where $\lambda(m)$ is a decreasing function of m that tends to zero at some maximum concentration M^* . The function $F(t)$ refers to the stochastic cytoneme attachment process - when a cytoneme attaches to a cell that has $M + 1$ packets, the number of packets decreases to M . The morphogen generation process could be simulated numerically by setting the probability of a new packet being developed in $(t, t + \delta t)$ equal to $1 - e^{-\lambda(m)t}$. However, we did not conduct further simulations along these lines as there is little experimental evidence with which to find appropriate parameter values for $\lambda(m)$. Thus, this is an area of future interest, and for situations when many cytonemes can attach to a producer cell, it may be necessary to consider producer cell dynamics as a limiting factor on the rate at which morphogens are distributed.

We will now turn to a discussion of diffusive transport mechanisms, followed by some comparisons between diffusion and cytoneme-based methods of distributing morphogens.

4 Diffusion vs cytonemes in a complex tissue environment

Both the Turing and positional-information mechanisms are based on diffusion in a homogeneous medium. The latter posits a mechanistic description of the form given below for establishment of the morphogen profile,

$$\begin{aligned} \frac{\partial c}{\partial t} &= D \frac{\partial^2 c}{\partial x^2} - kc & x \in (0, L) \\ -D \frac{\partial c}{\partial x}(x) &= j & x = 0 \\ -D \frac{\partial c}{\partial x}(x) &= 0 & x = L, \end{aligned} \quad (16)$$

but this rarely suffices to describe the detailed processes that are involved in biological tissues. For example, extracellular signals are detected by receptors, and this simple process adds terms for binding and release from the receptor to Equation 16, as well as a separate equation for the binding and release at the cell.

An example of a complex tissue in which patterning occurs is the widely-studied *Drosophila melanogaster* wing disc shown in Figure 11. The disc has two cell layers separated by a fluid lumen (Figure 11(A)), one a layer of columnar epithelial cells with the apical side at the lumen and a peripodial epithelium overlying the lumen [13](Figure 11(B)). The lateral membranes of adjacent cells are connected via two classes of junctions (ZAs and SJs) that separate the extracellular fluid into apical and baso-lateral layers [14, 19, 8] (details of the entire developmental process are given in [16]).

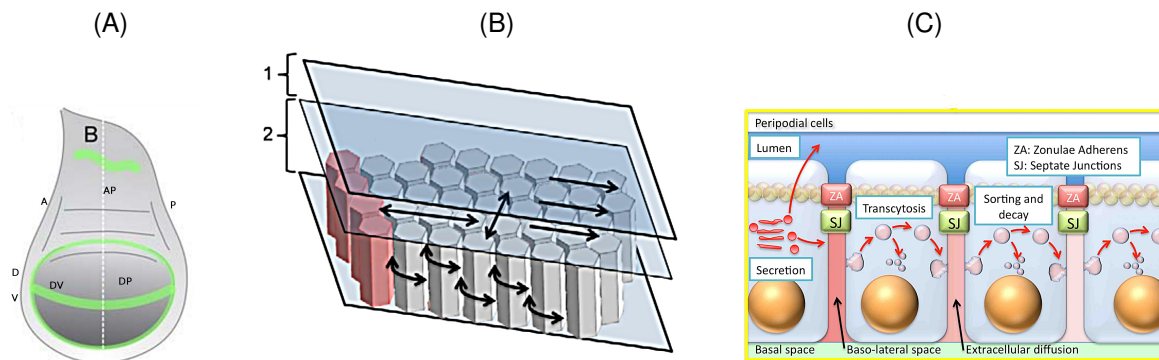


Fig 11. (A) The wing disc. (B) A section of the disc, showing the fluid luminal section (1), the hexagonal cells below (2), and the source of Dpp at the left along the AP boundary in (A). (C) A vertical cross-section showing the transport processes that affect the morphogen distribution [32].

The wing disc is perhaps the best understood system in which transport of a molecule – in this case the morphogen Dpp, involves a number of very distinct steps in a geometrically-complex tissue. The secretion of Dpp from a stripe of cells along the AP boundary, colored red in Figure 11(b) gives rise to a spatial distribution of Dpp transverse to the anterior-posterior midline of the disc, but how the distribution is established is still an open question. Three modes of transport have been identified in the disc – diffusion in the extracellular space, transcytosis, and transport via cytonemes [21, 38, 50]. While cytonemes are important in the transport of other morphogens [4], their role in Dpp transport is more ambiguous [2, 26]. Diffusion in the extracellular space can be free Brownian motion of a particle in solution, called 'free diffusion', or it may involve interactions with other factors, which is called 'facilitated diffusion' or 'restricted diffusion' [39, 38, 34].

Some experimental data shows a gradient of Dpp in the lumen and an apical layer of the columnar cells, but other results show that a graded Dpp distribution is found in the baso-lateral (BL) space [28, 18] and the luminal Dpp is uniformly distributed [13, 18]. Still others have shown that the majority of Dpp is in the intracellular space and the intracellular apical Dpp forms a long-range gradient [11, 21], but some have observed the opposite [3, 27, 41]. Experimentally-measured profiles of Dpp are usually described with a reaction-diffusion model such as Equation 16 [21, 47], but the estimate of the diffusion coefficient needed to

fit the data is much lower than usual values for free diffusion. Others [50] have measured a larger free coefficient for free diffusion in solution, and showed that the low value could be explained if receptor-mediated uptake and degradation are incorporated. However their analysis assumes a simple geometry corresponding to the luminal surface, but as indicated earlier, the geometry is quite complicated. Our next objective is to show how the structure of a complex tissue is reflected in the macroscopic parameters that appear in Equation 16.

4.1 From micro- to macro-parameters for diffusion and reaction

In a previous paper [42], hereafter referred to as **I**, we analyzed how microscale processes that are involved in transport in complex tissues are reflected in the macroscopic diffusion and decay terms in an equation such as Equation 16. Before providing an example to compare with the cytoneme transport, we briefly review some of the underlying ideas in that work.

The cellular level models are based upon continuous-time random walks (CTRWs). In a CTRW model, the key quantity of interest is the spatial distribution, $\mathbf{P}(\mathbf{x}, t|0)$ of particles at some time t , given that the particles move randomly via a series of jumps or transitions determined by a given stochastic model. Thus, let $\Psi(\mathbf{x}, t|\mathbf{y}, 0)$ be the joint probability density for a walker to instantaneously jump at t^- to a point \mathbf{x} after having starting at position \mathbf{y} at $t = 0^+$. From the space-time distribution of Ψ one can obtain a spatial jump distribution $T(\mathbf{x}, \mathbf{y})$ and the density of a waiting time distribution (WTD) $\phi(\mathbf{y}, t)$ as follows.

$$T(\mathbf{x}|\mathbf{y}) = \int_0^\infty \Psi(\mathbf{x}, \tau|\mathbf{y}, 0) d\tau, \quad \phi(\mathbf{y}, t) = \int_{\mathbb{R}^n} \Psi(\mathbf{x}, t|\mathbf{y}, 0) d\mathbf{x}.$$

Here T defines the probability of landing at \mathbf{x} , having started at \mathbf{y} , and $\phi(\mathbf{y}, t)dt$ is the probability of a jump in $(t, t + dt)$. From the latter one obtains the cumulative and complementary waiting-time distributions

$$\Phi(\mathbf{y}, t) = \int_0^t \phi(\mathbf{y}, s) ds = Pr\{\mathcal{T} \leq t\} \quad (17)$$

and

$$\hat{\Phi}(\mathbf{y}, t) = \int_t^\infty \phi(\mathbf{y}, s) ds = 1 - \Phi(t) = Pr\{\mathcal{T} \geq t\}. \quad (18)$$

In many contexts $\phi(\mathbf{y}, t)$ is independent of \mathbf{y} and $T(\mathbf{x}, \mathbf{y})$ is only a function of $\mathbf{x} - \mathbf{y}$, and with these simplifications one can obtain the following renewal equation for the spatial distribution of \mathbf{P} as

$$\mathbf{P}(\mathbf{x}, t|0) = \hat{\Phi}(t)\delta(\mathbf{x}) + \int_0^t \int_{\mathbb{R}^n} \phi(t - \tau)T(\mathbf{x}, \mathbf{y})\mathbf{P}(\mathbf{y}, \tau|0) d\mathbf{y} d\tau.$$

Since this equation is linear, we can define an equation for $N(\mathbf{x}, t)$, the probability distribution when the initial distribution is arbitrary. If we suppose that the WTD is Poisson-distributed, e.g. $\phi(t) = \lambda e^{-\lambda t}$, one can show that the system simplifies to

$$\frac{\partial N(\mathbf{x}, t)}{\partial t} = -\lambda N(\mathbf{x}, t) + \lambda \int_{\mathbb{R}^n} T(\mathbf{x}, \mathbf{y})N(\mathbf{y}, t) d\mathbf{y}.$$

This formulation assumes a translation-invariant continuum, but continuous time random walks can also be posed on lattices. A lattice is a countable set of points $\{\mathbf{X}\}$ in \mathbb{R}^d – called vertices of the lattice – whose positions are linear combinations of d linearly independent vectors with integer coefficients, endowed with a graph structure which specifies the connectivity of these points. The term ‘lattice’ also implies that the connectivity is the same for each point, e.g. in a square lattice, each point is connected to its neighboring points to the left, right, above, and below. In **I**, the lattice vertices are called junctions to distinguish them from secondary vertices that were introduced on the edges connecting junctions (*cf.* Figure 12). Lattices are of interest biologically since in many tissues cells arrange into lattice-like structures.

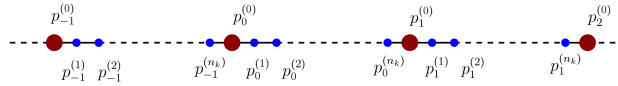


Fig 12. A diagram of a 1D lattice consisting of primary vertices or junctions (red) and secondary vertices (blue). The probabilities at the primary vertices are $p_i^{(0)}$, and the secondary vertices are denoted by $p_i^{(j)}$. Taken from [42] with permission.

In such settings the jump kernel $T(\mathbf{x} - \mathbf{y})$ is defined only for the vertices and can be thought of as a matrix operator. For a Poisson-distributed jump rate, the evolution equation on a general lattice is of the form

$$\frac{dP_i}{dt} = \lambda \sum_{j \in \mathcal{N}(i)} T_{i,j} \{P_j(t) - P_i(t)\}.$$

where $j \in \mathcal{N}(i)$ corresponds to a neighbor of i . To apply this in biological settings, we begin with a graph or lattice structure that defines the junctions, we introduce secondary vertices along edges connecting junctions, and we endow all secondary vertices with internal states as well. The internal states can describe binding, reaction, and other localized processes at each vertex, provided the transitions between states are linear (*cf.* I). The general form of the evolution equations is

$$\frac{d}{dt} N(\mathbf{X}, \tau) = -\lambda N(\mathbf{X}, t) + \lambda \int_0^t \sum_{\mathbf{X}' \in \mathcal{N}(\mathbf{X})} \mathbf{W}(\mathbf{X} - \mathbf{X}', t - \tau) N(\mathbf{X}', \tau) d\tau \quad (19)$$

where \mathbf{X} now contains the positions and the internal state at each position, and the λ is a diagonal matrix containing the exit rate for each state. The matrix-valued transition function \mathbf{W} is related to T as described in I, and since we assume that all processes have Poisson-distributed WTDs, $\mathbf{W}(\mathbf{X}, t) = \mathbf{W}_0(\mathbf{X})\delta(t)$ and \mathbf{W}_0 simply contains the rate constants for each possible transition between states.

The resulting stochastic process - with primary vertices, secondary vertices, and possible transitions between internal states - is called a multi-state CTRW. In general such processes can be quite complicated, since they contain many details about dynamics at a small-scale level, and the number of secondary vertices and internal states can be large. However, we are typically interested in assessing the evolution for longer time and space scales to determine the overall distribution of concentration or probability of a transported substance throughout a tissue that is many cell-lengths in size. Thus, the aim is to simplify such processes to obtain a reaction-diffusion system with fewer variables in which much of the local behavior has been averaged out, and in which the macro-scale coefficients reflect the small-scale processes via dependence of the macro-scale parameters on the microscale parameters. The outcome of this analysis is a reaction-diffusion system that hides much of the micro-level details in the diffusion coefficients and the kinetic parameters, and governs the evolution of concentrations on an entire edge. In one space dimension this equation can be used on any scale since the matching between edges simply involves continuity of the concentrations and fluxes at the junction, which by construction have no internal states. In other lattices the same equations apply on any edge and the same matching conditions must be satisfied, but the analysis is more complex due to the matching conditions, and this is the subject of a future publication.

In the next section we discuss a one-dimensional example that illustrates how micro-level parameters for several processes are reflected in macro-level parameters for an equation such as Equation 16.

4.1.1 Derivation of the macroscale equation for a transport model

Consider a line of cells, three of which are shown in Figure 13. separated by gap junctions⁶ The analysis that leads to the final result is long and complex, and the full details are given in I. Here we simply sketch the process as an example to be compared with transport via cytonemes later. We suppose that each cell is of width L and separated from its neighbors by fluid junctions of width δ . As shown in Fig. 13, we allow for

⁶An analysis of a simpler system like this in which cells were connected by porous junctions is given in [29].

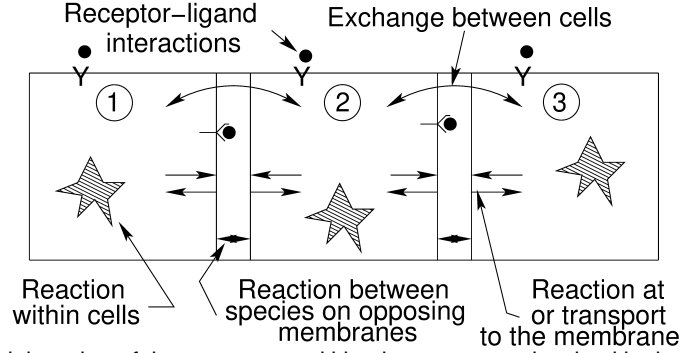


Fig 13. An elaboration of the transport and kinetics processes involved in the wing disc. In the analysis that follows not all processes shown are included. From [15] with permission.

internal reactions and degradation and transcytosis, and derive a macroscale equation that describes the overall process at large enough time and space scales. Within each cell there is diffusion, binding to and release from an immobile site, and degradation of the immobilized particle. The probability densities of states in cell i evolve according to the following equations.

$$\frac{\partial p_i^{(1)}}{\partial t} = D_{m,2} \frac{\partial^2 p_i^{(1)}}{\partial x^2} \quad (20)$$

$$\frac{\partial p_i^{(2,1)}}{\partial t} = D_{m,1} \frac{\partial^2 p_i^{(2,1)}}{\partial x^2} + k_- p_i^{(2,2)} - k_+ p_i^{(2,1)} \quad (21)$$

$$\frac{d p_i^{(2,2)}}{d t} = -k_- p_i^{(2,2)} + k_+ p_i^{(2,1)} - k_d p_i^{(2,2)}. \quad (22)$$

$$p_i^{(1)}(X_i, t) = p_i^{(2,1)}(X_i, t) \quad (23)$$

$$p_i^{(1)}(X_i + \delta, t) = p_{i+1}^{(2,1)}(X_i + \delta, t) \quad (24)$$

$$D_{m,1} \left. \frac{\partial p_i^{(1)}}{\partial x} \right|_{x=X_i} = D_{m,2} \left. \frac{\partial p_i^{(2,1)}}{\partial x} \right|_{x=X_i} \quad (25)$$

$$D_{m,1} \left. \frac{\partial p_i^{(1)}}{\partial x} \right|_{x=X_i+\delta} = D_{m,2} \left. \frac{\partial p_{i+1}^{(2,1)}}{\partial x} \right|_{x=X_i+\delta} \quad (26)$$

Here $p_i^{(1)}(x, t)$ is the probability density that a particle is located in the i th gap between the i^{th} and $(i+1)^{st}$ cells, and $p^{(2,1)}$ and $p^{(2,2)}$ represent the probabilities of mobile and bound states within a cell. The right-hand boundary of the i^{th} cell is at X_i , and the gap between cells is of length δ . The boundary conditions on $p_i^{(1)}$ and $p_i^{(2,1)}$ represent continuity conditions on the concentrations and fluxes for species that pass through the cell membrane, but do not bind to the membrane itself. Finally, to connect this with the previous lattice descriptions, we consider the right-hand cell membrane of each cell the junctions in this system. The above equations can be viewed as the reduction of a lattice description within cells to the reaction-diffusion equations shown.

The objective is to derive from the above equations a single reaction-diffusion equation in which the length scale $\epsilon \equiv \delta + L$ enters as a small quantity on the macroscopic length scale of interest. A detailed

analysis that is given in **I** leads to following equation to leading order as $\epsilon \rightarrow 0$.

$$\begin{aligned} \frac{\partial P(x, t)}{\partial t} &= -\frac{(1-\eta)\nu(0)}{\eta + (1-\eta)\nu'(0)} P(x, t) + \frac{1}{\left(\frac{(1-\eta)}{D_{m,2}} + \frac{\eta}{D_{m,1}}\right) (\eta + (1-\eta)\nu'(0))} \frac{\partial^2 P(x, t)}{\partial \xi^2} \\ &= -\left[\frac{(1-\eta)k_d k_+ (k_d + k_-)}{(k_d + k_-)^2 + (1-\eta)k_- k_+} \right] P(x, t) + \left[\frac{1}{\left(\frac{(1-\eta)}{D_{m,2}} + \frac{\eta}{D_{m,1}}\right) (\eta + (1-\eta) \left(1 + \frac{k_- k_+}{(k_d + k_-)^2}\right))} \right] \frac{\partial^2 P(x, t)}{\partial \xi^2} \\ &= -K_M P(x, t) + D_M \frac{\partial^2}{\partial \xi^2} P(x, t). \end{aligned} \quad (27)$$

The macroscale diffusion and degradation coefficients that emerge from the analysis are complex functions of the microscale parameters given by

$$K_M \equiv \frac{(1-\eta)k_d k_+ (k_d + k_-)}{(k_d + k_-)^2 + (1-\eta)k_- k_+}, \quad \text{and} \quad D_M \equiv \frac{1}{\left(\frac{(1-\eta)}{D_{m,2}} + \frac{\eta}{D_{m,1}}\right) (\eta + (1-\eta) \left(1 + \frac{k_- k_+}{(k_d + k_-)^2}\right))} \quad (28)$$

where $\eta \equiv \delta/L$, which remains constant in the limit $\epsilon \rightarrow 0$. Further details of these results are discussed in **I**, but it suffices to say that the derivation of the macroscale equations, though algebraically more complex, follows a general procedure that is applicable to many other problems. To start, we solve for the variables that rapidly equilibrate in terms of each other to reduce the number of equations. This typically yields effective WTDs that are FPT-distributions for transport between cells, for example, The splitting-probabilities and mean-waiting time are then computed, and these quantities are the only quantities that persist as $\epsilon \rightarrow 0$ in the macroscale limit. There also is typically a discrete-Laplacian type term that reduces to a coefficient (e.g. 1/2) times the continuum Laplacian.

Finally, we note that in any application, ϵ may be small but is still nonzero. Thus, it is necessary for sufficient time to have elapsed so that the waiting time for a single jump between adjacent cells is small compared with the time-scales of interest. Otherwise, the discrete cellular nature of the system will dominate and the continuum description will not be appropriate.

4.2 Comparison of diffusion with cytoneme transport in a regular hexagonal array of cells

4.2.1 Diffusive transport

The previous result shows that seemingly 'simple' macroscopic diffusion may in fact be a rather complex process when microscopic details are incorporated. In contrast, cytoneme-based transport can be much more direct, in that a PIT cytoneme deposits its entire load at one cell, and in this section we derive macroscopic equations for the evolution of a population of them. The example used focuses on morphogen spreading in cytoneme-based transport in a hexagonal lattice of cells that be thought of as a horizontal slice through the disc shown in Figure 11(C). Hexagonal lattices are of particular importance since many epithelial tissues can also be approximated to first-order as a system of hexagonally packed cells.

While not immediately obvious, regular hexagonal lattices can be constructed as an alternating pattern of two topologically distinct sets of points as in Figure 14. This connectivity structure arises since whereas all points are connected to three neighbors, and each point has two lateral connections, the blue (circle) points connect upwards to a red (square) point, whereas the red points connected downwards towards a blue point. Thus, the red and blue points are topologically distinct because they exhibit a mirror-image symmetry, but not translational symmetry. Said otherwise, while a square lattice in the plane is self-dual and thus translation invariant, the hexagonal lattice is not – its dual is a triangular lattice. In Figure 14 we denote the blue points as Type I, and the red points as Type II. It is important to note that this partitioning of the points stems from the topology of the hexagonal lattice, and does not imply that we must have different dynamics at the Type I and Type II points; the WTDs and all other physical properties associated with the Type I and Type

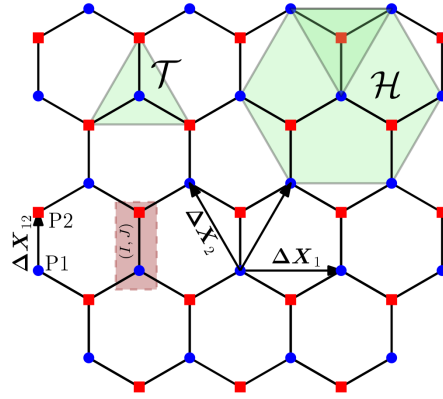


Fig 14. The terminology for the lattice. The red points (squares) attached solely to blue points (circles) and vice-versa. ΔX_1 and ΔX_2 specify the lattice directions, and ΔX_{12} is the displacement between type I and type II points. The green triangle, \mathcal{T} indicates the points attached to a Type I point, and the green hexagon, \mathcal{H} has as vertices the Type I points that are nearest to the Type I point at its center. Modified from [42].

II points are assumed equal in our models. For simplicity we only consider junction-to-junction steps in this section – the reader is invited to derive the equations when there are secondary vertices and internal states.

Since the hexagonal lattice has two distinct types of points, we have to consider jumps from Type I to Type II and jumps from Type II to Type I – there are no direct jumps that take a particle from a Type I point to another Type I point. If we let T_{12} indicate the transitions from Type II to Type I (see the shaded triangle labeled \mathcal{T} in Figure 14), and T_{21} as the transitions from Type I to Type II, we see that for diffusive transport, the two matrices are adjoints of one another. This is a consequence of the fact that the edges of a graph for a diffusion process are non-directed. Thus, the overall renewal equation for this system is of the form

$$\frac{d}{dt} \begin{pmatrix} P_1 \\ P_2 \end{pmatrix} = -\lambda \begin{pmatrix} P_1 \\ P_2 \end{pmatrix} + \lambda \begin{pmatrix} \mathbf{0} & T_{12} \\ T_{12}^* & \mathbf{0} \end{pmatrix} \begin{pmatrix} P_1 \\ P_2 \end{pmatrix}$$

where T_{12}^* is the Hermitian adjoint of T_{12} . With the alternating structure, it is convenient to solve for the Type II point probabilities in terms of the Type I points to obtain a single equation for the Type I points (see the shaded hexagon labeled \mathcal{H} in Figure 14). For simplicity, assume that the initial condition is concentrated on Type I points only, the general case is not difficult to obtain but involves more book-keeping which obfuscates the underlying method. This leads to a new equation of the form

$$\frac{d^2 P_1}{dt^2} + 2\lambda \frac{dP_1}{dt} = -\lambda^2 P_1 + \frac{\lambda^2}{9} \hat{T} P_1$$

where the new transition matrix is of the form $\hat{T} \equiv \mathbf{T}\mathbf{T}^*$.

By enumerating all of the possible jumps of Type I points to Type I points (*cf.* Figure 14), one can show that the right-hand side is equal to $(2/3)\lambda^2 \Delta_{\text{tri}} P_1$ where Δ_{tri} is the discrete Laplacian for a triangular lattice with spacing $\sqrt{3}L$ (see [31] for an explicit expression for the Laplacian). The $\sqrt{3}L$ factor arises since resultant length of any two adjacent edges of the hexagonal lattice is $\sqrt{3}$ times the length of the individual edges.⁷

Now that the lattice topology has been described, it is possible to obtain a macroscale limit equation. In the asymptotic limit of many jumps, a particle has generally traveled a distance many times greater than L , and thus, we want to consider L as a small parameter for our asymptotic analysis. We also consider that in

⁷The fact that the triangle-lattice spatial transition operator appears is result is a consequence of the duality between hexagonal and triangular lattices, and can be seen in Figure 14 by noting that each Type I (or Type II) point has six nearest-neighbor points of the same type, separated by distances $\pm\Delta X_i$ for $i = 1, 2$ and $\pm(\Delta X_1 + \Delta X_2)$. In fact, we see that if we add points to the center of each hexagon, and connect adjacent hexagons, we obtain the triangle lattice, as shown in the darker triangle in Figure 14). Given this observation, it is possible to consider more sophisticated problems with both internal and external transport by explicitly adding these center-points into the system and connecting them to the honeycomb lattice vertices via the addition of new edges.

this case, the Laplace-transformed memory kernel $\tilde{\Gamma} = s/\lambda^2 + 2/\lambda$ cf. [42]. Computing the Taylor-expansion of the discrete Laplacian that arises here we, we obtain

$$[\Delta_{\text{tri}}]P(\mathbf{x}) = 3L^2\Delta P(\mathbf{x}) + O(L^4\Delta\Delta P).$$

Further, since we set $\lambda \sim D/L^2$, we obtain

$$\tilde{\Gamma} = 2\frac{L^2}{D} + s\frac{L^4}{D^2}.$$

At leading order, the L^4 term drops out and we obtain a diffusion equation,

$$\frac{\partial p}{\partial t} = D\Delta p + O(L^2)$$

While this result is still formal since we have not proven that the higher order terms vanish, it is possible to show this result rigorously by conducting an eigenvalue analysis to show that the eigenvalues corresponding to fast modes (associated with differences in the concentrations of the Type I and Type II points) vanish to $-\infty$ as $L \rightarrow 0$. The fact that a telegrapher approximation never results is similar to the result in [30]. Since there is only a single time-scale (e.g. the system is time homogeneous), the initial 'ballistic' regime, characteristic of the telegraph's equation, disappears as $L \rightarrow 0$.

Finally, we remark on what happens to P_2 in this limit. In the small- ϵ limit, a similar Taylor series expansion would show that P_2 reduces to a local average of P_1 . When P_1 is sufficiently smooth, local averaging reduces to the identity operator as L shrinks to zero. Thus, $P_2 = P_1$ to leading order at the macroscale.

While we do not explore the diffusion case further, we do note that if a more complicated model were proposed for transport along each edge, a similar approach can be used, but as in the previous section, the diffusion coefficient becomes for more complicated.

4.2.2 Transport via PIT cytonemes

To compare diffusive transport and transport by cytonemes on a hexagonal lattice, we derive a macroscale equation for a cytoneme transfer process of PIT type through the lattice. We will assume that, as with the diffusive transport described in the previous section, the cytonemes must traverse the fluid gaps between cells, and thus move along the hexagonal lattice. However, the movement of a tip is different in that the cytonemes extend and do not reverse direction until they reach a target and deliver their morphogen bolus.

While each cytoneme travels without reversal, it can 'die' along an edge in that we ignore it after it delivers its cargo to a cell. Upon reaching a junction, cytonemes cannot reverse, but can choose to travel along one of the two other edges that intersect that trijunction. While there no reversal, cytonemes could potentially travel in a loop by making 5 right turns or 5 left turns in a row. To eliminate this possibility, which may be biologically irrelevant, we assume that cytonemes travel in the direction of greater x in 2D whenever they reach a junction. Under this condition, a typical cytoneme path is as shown in Figure 15. As mentioned earlier, movement may be guided by a signal emanating from receiver cells, which would automatically decrease the probability of loops in populations of cytonemes.

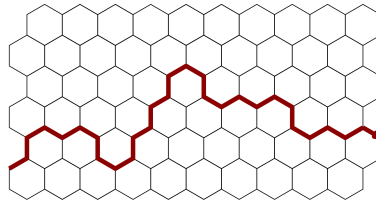


Fig 15. The typical path of a cytoneme under the condition that it can move vertically, but always tends towards the right.

Since there are two topological types of junctions, this again leads to a 2-state system. We will assume here that the lattice is aligned as in Figure 14, and that all cytonemes move in the $+x$ -direction except when on the vertical edges. We then have at each step a probability of αp of continuing to the right, a probability of $\alpha(1-p)$ making a vertical transition, and finally a probability of $(1-\alpha)$ for decay (see Figure 16).

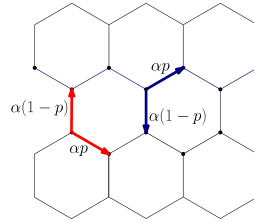


Fig 16. Spatial jump probabilities for a cytoneme arriving departing from a Type I (blue) or Type II (red) point. The two parameters, $p, \alpha \in (0, 1)$.

This system can be written at an arbitrary lattice point \mathbf{x} as

$$\frac{d}{dt} \begin{pmatrix} P_I(\mathbf{x}) \\ P_{II}(\mathbf{x}) \end{pmatrix} = -\lambda \begin{pmatrix} P_I(\mathbf{x}) \\ P_{II}(\mathbf{x}) \end{pmatrix} + \lambda \alpha p \begin{pmatrix} 0 & S_{-1} \\ S_{-2} & 0 \end{pmatrix} \begin{pmatrix} P_I(\mathbf{x}) \\ P_{II}(\mathbf{x}) \end{pmatrix} + \lambda \alpha (1-p) \begin{pmatrix} 0 & 1 \\ 1 & 0 \end{pmatrix} \begin{pmatrix} P_I(\mathbf{x}) \\ P_{II}(\mathbf{x}) \end{pmatrix} \quad (29)$$

where $[S_{\pm i}P](\mathbf{x}) = P(\mathbf{x} \pm \delta \mathbf{x}_i)$ are shift operators that allow us to specify connections between adjacent points on the lattice. While it is possible to invert this 2×2 system directly, we again reduce the system to a single equation in order to determine the macroscopic equation that results from this system in the limit when the edge length $L \rightarrow 0$. We do not expect that the distinction between Type I and Type II vertices will be significant at the macroscale, and therefore we solve for the type II probabilities in terms of the type I probabilities to obtain

$$\frac{\partial^2 P_I}{\partial t^2} + 2\lambda \frac{\partial P_I}{\partial t} = (\lambda^2 \alpha^2 (1-p)^2 - \lambda^2) P_I + \lambda^2 \alpha^2 p (1-p) [P_I(\mathbf{x} - \delta \mathbf{x}_1) + P_I(\mathbf{x} - \delta \mathbf{x}_2)] + \lambda^2 \alpha^2 p^2 P(\mathbf{x} - \delta \mathbf{x}_1 - \delta \mathbf{x}_2).$$

where λ^{-1} is the mean time to traverse a single edge. Since the motion is advective, $\lambda^{-1} \sim v/L$. We also set $\alpha \sim (1 - k_d L)$ so that decay is not too fast to obtain a macroscale equation. The constant, k_d will be closely related to the macroscale degradation coefficient. Then, in the limit $L \rightarrow 0$ the equation that results is

$$\frac{\partial P}{\partial t} + \frac{vp}{2} \frac{\partial P}{\partial x} = -(vk_d)P.$$

What is particularly striking about this equation is that there is no flux term in the y direction at large scales, despite the fact that at a microscopic scale, cytonemes can make vertical jumps. The reason is that while cytoneme makes vertical jumps up and down, on average these vertical fluctuations cancel out (and thus spreading along the y -axis is not of leading order), and thus do not appear in the macroscopic equations.

Thus, we see that in the diffusive transport case, we obtain a diffusion-reaction equation with coefficients that depend on the microscale model, whereas cytoneme-transport gives a one-dimensional advection-reaction equation. To compare these, we consider a stripe of producer cells, and for simplicity, assume that in the diffusion case, there are reflecting boundary conditions at the top and bottom of the tissue. If we assume uniformity in the y -direction, then the 2-dimensional diffusion reduces to a one-dimensional diffusion equation with a source at $x = 0$. Under these simplifications, we can compare the diffusion and cytoneme-based models.

To make a fair comparison, we suppose that in each case, there is a specified flux J at $x = 0$ in both cases. For conciseness, we also set v and D equal to the macroscale diffusion and reaction coefficients obtained above, and λ equal to the degradation coefficients determined above. Then, for cytoneme-mediated transport, we have $J = vP(0, t)$, and for diffusion, $J = -DP_x|_{x=0}$. The resulting

solutions to this 1-dimensional problem are then given as

$$P(x, t) = \frac{J}{v} H(t - x/v) e^{-\frac{\lambda}{v}x}$$

$$P(x, t) = \frac{J}{2\sqrt{\lambda D}} \left[e^{-\sqrt{\lambda/D}x} \operatorname{Erfc} \left(\frac{x - 2t\sqrt{D\lambda}}{2\sqrt{Dt}} \right) - e^{\sqrt{\lambda/D}x} \operatorname{Erfc} \left(\frac{x + 2t\sqrt{D\lambda}}{2\sqrt{Dt}} \right) \right]. \quad (30)$$

Several observations can be made from these solutions. Firstly, when $D = 1\mu\text{m}^2/\text{sec}$ and $v = 1\mu\text{m}/\text{sec}$ with $\lambda = 1/\text{sec}$, both solutions are equivalent in the limit $t \rightarrow \infty$ suggesting that in biological situations where the diffusivity, advective velocity, and reaction rates are of roughly equal importance, either strategy could be applied in theory. On the other hand, the dynamics are quite different. Under diffusion, the concentration distribution gradually increases everywhere in space, whereas under advection, the concentration distribution is unfolded over time, but once it is set, does not change.

When λ is allowed to vary, we see that for $\lambda < 1$, diffusion leads to a broader distribution relative to advection, whereas when $\lambda > 1$, the opposite occurs. Both situations have potential roles biologically, for instance, if it is important that distant cells be reached, then the strategy that yields a greater extent of travel might be more useful, whereas, if cells are detecting the gradient of a substance, than the shorter, and hence more sharply peaked distribution might be more effective at achieving biological goals.

5 Discussion

Herein we have developed deterministic and stochastic models of transport by cytonemes, both when the receiver cell searches for a producer cell, and when the producer cell extends cytonemes to deliver cargo to receivers. In simple models analytical solutions are attainable, and the complete spatiotemporal dependence of the morphogen concentration has been obtained. A key quantity that arises is the rate μ/v of the cytoneme halting rate compared with its velocity. This parameter controls the steepness of the cytoneme concentration field, and hence how far morphogen can spread.

We then discussed the generalization of the simple models to include stochastic cytoneme generation rates, and discussed some analytical results concerning the statistics of morphogen received at a given cell in this case. A key point in these models is that since cytonemes are presumed not to interact amongst themselves, the position of the receiving cell shows up merely as a parameter in the models. It would be of interest to ascertain experimentally whether or not nearby cytonemes can interact, and whether this has implications for morphogen transport.

We next considered a stochastic simulation approach for more complex models. While many of the features of the simpler model is present in this case, the basic stochastic models are easy to extend to include features such as feedback mechanisms whereby cells turn off cytoneme generation after receiving enough morphogen. There are many further extensions that can be applied here - notably, it is straightforward to include more complicated morphogen extension and retraction steps, and the possibility of a variable morphogen bolus size and even the ability to consider dynamic morphogen transport along cytonemes that are attached to a producer cell.

Finally, we discussed how cell-level models that include details of the diffusive or cytoneme-mediated transport processes can be upscaled to obtain tissue-level macroscale equations. These macroscale equations take on much simpler forms, but have coefficients that depend in complex ways on the microscale details of the transport procedures. At this level, we discussed a simple comparison between diffusive transport and cytoneme-mediated transport. We found that either model can yield the same distribution of morphogen after some time, but that the dynamics of the approach to the longer-term morphogen distribution differ between the modes. This suggests that understanding the importance of diffusion and cytoneme-based transport to morphogen spreading may require not only analysis of 'steady-state' distributions of morphogen, but also the dynamics of the morphogen concentration field over time.

6 Acknowledgments

This work was supported in part by NSF Grants DMS # 178743 and 185357.

References

1. A. Aguirre-Tamaral and I. Guerrero, Improving the understanding of cytoneme-mediated morphogen gradients by in silico modeling, *PLoS Computational Biology*, **17** (2021), e1009245.
2. T. Akiyama and M. C. Gibson, Morphogen transport: theoretical and experimental controversies, *Wiley Interdisciplinary Reviews: Developmental Biology*, **4** (2015), 99–112.
3. T. Y. Belenkaya, C. Han, D. Yan, R. J. Opoka, M. Khodoun, H. Liu and X. Lin, *Drosophila* dpp morphogen movement is independent of dynamin-mediated endocytosis but regulated by the glypican members of heparan sulfate proteoglycans, *Cell*, **119** (2004), 231–244.
4. M. Bischoff, A. Gradilla, I. Seijo, G. Andrés, C. Rodríguez-Navas, L. González-Méndez and I. Guerrero, Cytonemes are required for the establishment of a normal hedgehog morphogen gradient in *Drosophila* epithelia, *Nat. Cell Biol.*
5. P. C. Bressloff and H. Kim, Bidirectional transport model of morphogen gradient formation via cytonemes, *Physical Biology*, **15** (2018), 026010.
6. P. C. Bressloff and H. Kim, Search-and-capture model of cytoneme-mediated morphogen gradient formation, *Physical Review E*, **99** (2019), 052401.
7. C. M. Child, *Patterns and Problems of Development.*, University of Chicago press, Chicago, 1941.
8. K.-W. Choi, Upstream paths for Hippo signaling in *Drosophila* organ development, *BMB Reports*, **51** (2018), 134.
9. D. R. Cox, *Renewal Theory*, Methuen, 1962.
10. C. A. Daly, E. T. Hall and S. K. Ogden, Regulatory mechanisms of cytoneme-based morphogen transport, *Cellular and Molecular Life Sciences*, **79** (2022), 1–20.
11. E. V. Entchev, A. Schwabedissen and M. González-Gaitán, Gradient formation of the TGF- β homolog dpp, *Cell*, **103** (2000), 981–992.
12. S. Fancher and A. Mugler, Diffusion vs. direct transport in the precision of morphogen readout, *Elife*, **9** (2020), e58981.
13. M. C. Gibson, D. A. Lehman and G. Schubiger, Lumenal transmission of decapentaplegic in *Drosophila* imaginal discs., *Dev Cell*, **3** (2002), 451–60.
14. W. T. Gibson and M. C. Gibson, Cell topology, geometry, and morphogenesis in proliferating epithelia, *Curr. Topics Dev. Biol.*, **89** (2009), 87–114.
15. J. Gou, L. Lin and H. G. Othmer, A model for the Hippo pathway in the *Drosophila* wing disc, *Biophys. J.*, **115** (2018), 737–747, PMID: 30041810.
16. J. Gou, J. A. Stotsky and H. G. Othmer, Growth control in the *Drosophila* wing disk, *Wiley Interdisciplinary Reviews: Systems Biology and Medicine*, e1478.
17. E. T. Hall, M. E. Dillard, D. P. Stewart, Y. Zhang, B. Wagner, R. M. Levine, S. M. Pruetz-Miller, A. Sykes, J. Temirov, R. E. Cheney et al., Cytoneme delivery of Sonic Hedgehog from ligand-producing cells requires myosin 10 and a Dispatched-boc/cdon co-receptor complex, *Elife*, **10** (2021), e61432.

18. S. Harmansa, I. Alborelli, D. Bieli, E. Caussinus and M. Affolter, A nanobody-based toolset to investigate the role of protein localization and dispersal in *Drosophila*, *Elife*, **6** (2017), e22549.
19. T. J. Harris and U. Tepass, Adherens junctions: from molecules to morphogenesis, *Nat. Revs. Mol. Cell Biol.*, **11** (2010), 502–514.
20. T. Hillen and K. J. Painter, A user's guide to PDE models for chemotaxis, *J. Math. Biol.*, **58** (2009), 183–217.
21. A. Kicheva, P. Pantazis, T. Bollenbach, Y. Kalaidzidis, T. Bittig, F. Jülicher and M. Gonzalez-Gaitan, Kinetics of morphogen gradient formation, *Science*, **315** (2007), 521–525.
22. H. Kim and P. C. Bressloff, Direct vs. synaptic coupling in a mathematical model of cytoneme-based morphogen gradient formation, *SIAM Journal on Applied Mathematics*, **78** (2018), 2323–2347.
23. O. Korenkova, A. Pepe and C. Zurzolo, Fine intercellular connections in development: Tnts, cytonemes, or intercellular bridges?, *Cell Stress*, **4** (2020), 30.
24. T. B. Kornberg, Cytonemes extend their reach, *The EMBO journal*, **32** (2013), 1658–1659.
25. J. Masoliver, J. M. Porra and G. H. Weiss, Solution to the telegrapher's equation in the presence of reflecting and partly reflecting boundaries, *Physical Review E*, **48** (1993), 939.
26. S. Matsuda, S. Harmansa and M. Affolter, Bmp morphogen gradients in flies, *Cytokine & growth factor reviews*, **27** (2016), 119–127.
27. P. Müller, K. W. Rogers, R. Y. Shuizi, M. Brand and A. F. Schier, Morphogen transport, *Development*, **140** (2013), 1621–1638.
28. M. G. Mundt, *Characterization of a Unique Basolateral Targeting Domain in the Drosophila TGF- β Type II Receptor Punt*, Master's thesis, University of Minnesota, 2013.
29. H. G. Othmer, A continuum model for coupled cells, *J. Math. Biol.*, **17** (1983), 351–369.
30. H. G. Othmer, S. R. Dunbar and W. Alt, Models of dispersal in biological systems., *J. Math. Biol.*, **26** (1988), 263–298.
31. H. G. Othmer and L. E. Scriven, Instability and dynamic pattern in cellular networks, *J. Theor. Biol.*, **32** (1971), 507–537.
32. H. G. Othmer, K. Painter, D. Umulis and C. Xue, The intersection of theory and application in biological pattern formation, *Math. Mod. Nat. Phenom.*, **4** (2009), 3–82.
33. F.-A. Ramírez-Weber and T. B. Kornberg, Cytonemes: cellular processes that project to the principal signaling center in drosophila imaginal discs, *Cell*, **97** (1999), 599–607.
34. S. Restrepo, J. J. Zartman and K. Basler, Coordination of patterning and growth by the morphogen dpp, *Curr. Biol.*, **24** (2014), R245–R255.
35. B. L. Ricca and R. S. Rock, The stepping pattern of myosin X is adapted for processive motility on bundled actin, *Biophysical Journal*, **99** (2010), 1818–1826.
36. S. M. Ross, *Stochastic Processes*, 2nd edition, Wiley New York, 1996.
37. D. Routledge and S. Scholpp, Mechanisms of intercellular Wnt transport, *Development*, **146** (2019), dev176073.
38. G. Schwank, S. Dalessi, S. Yang, R. Yagi, A. M. de Lachapelle, M. Affolter, S. Bergmann and K. Basler, Formation of the long range Dpp morphogen gradient, *PLoS Biology*, **9** (2011), e1001111.

39. O. Shimmi, D. Umulis, H. G. Othmer and M. B. O'Connor, Facilitated transport of a Dpp/Scw heterodimer by Sog/Tsg leads to robust patterning of the *Drosophila* blastoderm embryo, *Cell*, **120** (2005), 873–86.
40. E. Stanganello and S. Scholpp, Role of cytonemes in Wnt transport, *Journal of cell science*, **129** (2016), 665–672.
41. K. S. Stapornwongkul and J.-P. Vincent, Generation of extracellular morphogen gradients: the case for diffusion, *Nature Reviews Genetics*, **22** (2021), 393–411.
42. J. A. Stotsky, J. Gou and H. G. Othmer, A random walk approach to transport in tissues and complex media: from microscale descriptions to macroscale models, *Bull. Math. Biology*, **83** (2021), 1–84.
43. H. Teimouri and A. B. Kolomeisky, New model for understanding mechanisms of biological signaling: direct transport via cytonemes, *J. Physical Chemistry Letters*, **7** (2016), 180–185.
44. A. M. Turing, The chemical basis of morphogenesis, *Phil. Trans. R. Soc. London*, **237** (1952), 37–72.
45. D. M. Umulis and H. G. Othmer, Mechanisms of scaling in pattern formation, *Development*, **140** (2013), 4830–4843.
46. G. Vasilopoulos and K. J. Painter, Pattern formation in discrete cell tissues under long range filopodia-based direct cell to cell contact, *Math. Biosciences*, **273** (2016), 1–15.
47. O. Wartlick, P. Mumcu, F. Jülicher and M. Gonzalez-Gaitan, Understanding morphogenetic growth control – lessons from flies, *Nat. Rev. Mol. Cell Biol.*, **12** (2011), 594–604.
48. L. Wolpert, Positional information and the spatial pattern of cellular differentiation, *J. Theor. Biol.*, **25** (1969), 1–47.
49. Y. M. Yamashita, M. Inaba and M. Buszczak, Specialized intercellular communications via cytonemes and nanotubes, *Ann. Rev. Cell and Developmental Biology*, **34** (2018), 59–84.
50. S. Zhou, W.-C. Lo, J. L. Suhalim, M. A. Digman, E. Gratton, Q. Nie and A. D. Lander, Free extracellular diffusion creates the Dpp morphogen gradient of the *Drosophila* wing disc, *Curr. Biol.*, **22** (2012), 668–675.

7 Appendices

7.1 Computation of FPT for cytonemes with a resting phase

Let us consider the computation of the FPT for the model of cytonemes extending and retraction with a resting phase. This is an example of an alternating renewal process, and the solution for the FPT is computable via the use of Laplace-transforms.

The governing equations for this model are described in Section 2.1 and Equations (7). After Laplace transformation, and assuming an initial condition that a cytoneme is generated at x_0 at $t = 0$, we obtain an algebraic system for the Laplace-transformed quantities

$$\begin{aligned}
 s\tilde{p}_e - v\tilde{p}_{e,x} &= -\lambda_m\tilde{p}_e + \lambda_r\tilde{r}_1 + \frac{1}{v}\delta(x - x_0) \\
 s\tilde{r}_1 &= \lambda_m\tilde{p}_e - \lambda_r\tilde{r}_1 \\
 s\tilde{P}_a &= v\tilde{p}_e(0, s) - \mu_d\tilde{P}_a \\
 s\tilde{p}_r + v\tilde{p}_{r,x} &= -\lambda_m\tilde{p}_r + \lambda_r\tilde{r}_2 + \delta(x)\frac{\mu_d}{v}\tilde{P}_a \\
 s\tilde{r}_2 &= \lambda_m\tilde{p}_r - \lambda_r\tilde{r}_2
 \end{aligned} \tag{31}$$

For the FPT problems, we are interested in the quantity $vp_r(x_0, t)$, which can be found from above as

$$\tilde{f}(s|x_0) = \frac{\mu_d}{s + \mu_d} e^{-\frac{2x_0}{v}(s + \lambda_m - \frac{\lambda_m \lambda_r}{s + \lambda_r})}$$

To invert this, first note that the product of Laplace-transform domain quantities leads to their convolution in real-time and that the inverse transform of $e^{-as}\tilde{g}(s)$ leads to step functions, $H(t-a)g(t-a)$ where $g(t)$ is an arbitrary function whose Laplace-transform is sufficiently well-behaved. With these result, let us consider just the inverse transform of

$$e^{-\alpha/(s+\lambda_r)}.$$

We can further use the Laplace-transform shift formula and just consider $e^{-\alpha/s}$. While the inversion integral is involved, it can be shown (or looked up in a table), that the inverse transform is

$$\sqrt{\frac{\alpha}{t}} I_1(2\sqrt{\alpha t}) + \delta(t)$$

where $I_1(\alpha)$ is the modified Bessel-function of the first kind of order 1. Applied to our case, we obtain an inverse

$$f(t|x_0) = \int_0^t \left[\mu_d e^{-\mu_d(t-\tau)} H\left(\tau - \frac{2x_0}{v}\right) \left[e^{-(\tau + \frac{x_0}{v})\lambda_m} \sqrt{\frac{c}{(\tau - \frac{2x_0}{v})}} I_1\left(2\sqrt{c\left(\tau - \frac{2x_0}{v}\right)}\right) + \delta\left(\tau - \frac{2x_0}{v}\right) \right] \right] d\tau$$

with $c = 2\lambda_m \lambda_r x_0 / v$. The convolution integral that results does not appear to have any obvious simplification, but could be numerically evaluated if needed. On the other hand, from the Laplace-transformed result, it is straightforward to compute moments with respect to t by differentiating $\tilde{f}(s)$ at $s = 0$. For instance,

$$\langle t \rangle = \frac{1}{\mu_d} + \frac{2x_0}{v} \left(1 + \frac{\lambda_m}{\lambda_r} \right)$$

Notice that the two terms, $1/\mu_d$ and the velocity dependent term essentially account for 1) the cytoneme to be attached to the producer cell, and 2) the time it takes to go out and come back.

The variance can be computed by taking the second derivative at $s = 0$ and subtracting $\langle t \rangle^2$. This leads to

$$\sigma^2(t) = \langle (t - \langle t \rangle)^2 \rangle = \frac{1}{\mu_d^2} + \frac{4x_0}{v} \frac{\lambda_m}{\lambda_r^2}$$

which again, has components due to the variance of waiting while attached, and of the time it takes to travel to and from the producer cells.

7.2 Simplification of double sum for the composite process

We found in Section 3.2 that the distribution function for sums of Bernoulli variables that are themselves dependent on a Poisson process results in a rather simple form, namely that the the resulting distribution is exponentially distributed with a time-dependent rate-parameter.

Here, we show how this may be computed starting from Equation (15), reproduced below

$$\mathbb{P} \left[\sum_{i=1}^{N(t)} R(t|t_i) - N_r \geq 0 \right] = \sum_{n=0}^{\infty} p_n(t) \mathbb{P}_n \left[\sum_{i=1}^n R(t|t_i) > N_r \right].$$

We assume that each $R_i(t|t_i)$ is itself a random variable, and that all the R 's are i.i.d. and take on values of 0 and 1 with some probability for each $t > t_i$. At time t , let $r(t|0)dt$ be the probability that R goes from 0 to 1 in the interval $(t, t + dt)$. As an example, this could be the probability that a cytoneme which started at $t = 0$ returns to the cell it started at around time t . Since the t_i are also random times, we can define a density for the probability of obtaining N_r successes (e.g. R goes from 0 to 1) in the intervals $(t_1, t_1 + dt)$, $(t_2, t_2 + dt)$,

..., $(t_n, t_n + dt)$. This is equal to the sum over all possible combinations of j out of n R_i 's becoming successful at t . Since the R_i 's are all i.i.d., this can be written as

$$P(t, N_r | n, \{t_1, \dots, t_n\}) = \sum_{A \in V_{N_r, n}} \prod_{i \in A} r(t|t_i) \prod_{j \in A^c} (1 - r(t|t_j))$$

where $V_{N_r, n}$ is the set of all combinations of N_r elements of $\{t_1, \dots, t_n\}$, $A = \{t_{a_1}, \dots, t_{a_{N_r}}\}$ is an element of $V_{N_r, n}$, and A^c is the complement of A . This appears quite complicated at first glance since each of the Bernoulli variables has a potentially distinct success probability at t since each t_i is generally distinct from the others. However, we next want to take the expectation over all of the t_i to find the probability of having N_r successes at any combination of times prior to t . To integrate, we note that due to independence, in each term of the sum, each $t_i \in \{t_1, \dots, t_n\}$ appears precisely once, and upon taking the expectation of any particular element, $A \in V_{N_r, n}$, we obtain

$$\begin{aligned} \mathbb{E}_1 \left[\prod_{i \in A} r(t|t_i) \prod_{j \in A^c} (1 - r(t|t_j)) \right] &= \frac{1}{t^n} \underbrace{\int_0^t \dots \int_0^t}_{n \text{ times}} \left[\prod_{i \in A} r(t|t_i) \prod_{j \in A^c} (1 - r(t|t_j)) \right] dt_1 dt_2 \dots dt_n \\ &= \prod_{i \in A} \mathbb{E}_1[r(t|\cdot)] \prod_{j \in A^c} (1 - \mathbb{E}_1[r(t|\cdot)]) = \mathbb{E}_1[r(t|\cdot)]^{N_r} (1 - \mathbb{E}_1[r(t|\cdot)])^{n - N_r} \end{aligned} \quad (32)$$

For short-hand, define $\bar{r}(t) = \mathbb{E}_1[r(t|\cdot)]$. The cardinality of $V_{N_r, n}$ is the set of all possible combinations containing N_r successes out of n tried, which is just $\binom{n}{N_r}$, thus leading to

$$\mathbb{E} [P(t, N_r | n \{t_1, \dots, t_n\})] = P(t, N_r | n) = \binom{n}{N_r} \bar{r}(t)^{N_r} (1 - \bar{r}(t))^{n - N_r}.$$

In general, we are interested in the probability of $\sum_{i=1}^n R_i(t|t_i) \geq N_r$, thus we must sum over $j = N_r$ to $j = n$, e.g.

$$\sum_{j=N_r}^n \binom{n}{j} \bar{r}(t)^j (1 - \bar{r}(t))^{n-j}.$$

and finally compute the expectation over n . For a Poisson process with constant rate, this leads to

$$\mathbb{P} \left[\sum_{i=1}^{N(t)} R(t|t_i) - N_r \geq 0 \right] = \sum_{n=0}^{\infty} e^{-\lambda t} \frac{(\lambda t)^n}{n!} \sum_{j=N_r}^n \binom{n}{j} \bar{r}(t)^j (1 - \bar{r}(t))^{n-j}$$

To compute this sum, it is best to interchange the order of summation between j and n . Note that in each term it is always true that, $n \geq j$. After interchanging the order and finding the appropriate bounds on the sums, we obtain

$$\mathbb{P} \left[\sum_{i=1}^{N(t)} R(t|t_i) - N_r \geq 0 \right] = \sum_{j=N_r}^{\infty} \sum_{n=j}^{\infty} e^{-\lambda t} \frac{(\lambda t)^n}{n!} \binom{n}{j} \bar{r}(t)^j (1 - \bar{r}(t))^{n-j}$$

Further simplification is done by defining $m = n - j$ yielding

$$\mathbb{P} \left[\sum_{i=1}^{N(t)} R(t|t_i) - N_r \geq 0 \right] = e^{-\lambda t \bar{r}(t)} \sum_{j=N_r}^{\infty} \frac{(\lambda t \bar{r}(t))^j}{j!} = 1 - e^{-\lambda t \bar{r}(t)} \sum_{j=0}^{N_r-1} \frac{(\lambda t \bar{r}(t))^j}{j!}$$

We see that this happens to be the cumulative sum for a exponentially distributed discrete variable. Furthermore, it is known that the sum can be written in 'closed' form in terms of the upper incomplete Gamma-function: $\Gamma(N_r, \lambda t \bar{r}(t))$,

$$\mathbb{P} \left[\sum_{i=1}^{N(t)} R_i(t|t_i) - N_r \geq 0 \right] = \frac{1}{(N_r - 1)!} \int_{\lambda t \bar{r}(t)}^{\infty} z^{N_r - 1} e^{-z} dz.$$

Note that regardless of how complex the dynamics of $R_i(t|t_i)$ are, this result is a consequence of the independence of the motion of all of the cytonemes. It is of future interest to determine whether similar results may be obtainable when there is some dependence between cytonemes either due to spatial interactions, or when the cytoneme generation process is not a Poisson process.